REFLECTION SEISMIC DATA ACQUISITION AND PROCESSING FOR ENHANCED INTERPRETATION OF HIGH RESOLUTION OBJECTIVES

by

KENNETH WILLIAM "WEISENBURGER"

THESIS submitted to the Faculty of the
Virginia Polytechnic Institute and State University
in partial fulfillment of the requirements for the degree of
MASTER OF SCIENCE
in
GEOPHYSICS

APPROVED:

J. K. COSTAIN, CHAIRMAN

C. CORUH

E. S. ROBINSON

AUGUST , 1985

Blacksburg, Virginia

REFLECTION SEISMIC DATA ACQUISITION AND PROCESSING

FOR ENHANCED INTERPRETATION OF

HIGH RESOLUTION OBJECTIVES

by

KENNETH WILLIAM WEISENBURGER

J. K. COSTAIN, CHAIRMAN

GEOPHYSICS

(ABSTRACT)

Reflection seismic data were acquired (by CONOCO, Inc.) which targeted known channel interuption of an upper Pennsylvanian coal seam (Herrin #6) in the Illinois basin. The data were reprocessedand interpreted by the Regional Geophysics Laboratory, Virginia Tech. Conventional geophysical techniques involving field acquisition and data processing were modified to enhance and maintain high frequency content in the signal bandwidth. Single sweep processing was employed to increase spatial sampling density and reduce low pass filtering associated with the array response. Whitening of the signal bandwidth was accomplished using Vibroseis whitening (VSW) and stretched automatic gain control (SAGC). A zero-phase wavelet-shaping filter was used to optimize the waveform length allowing a thinner depositional sequence to be resolved.

The high resolution data acquisition and processing led to an interpreted section which shows cyclic deposition in a deltaic environment. Complex channel development interrupted underlying sediments including the Herrin coal seam complex. Contrary to previous interpretations of

channel development in the study area by Chapman and others (1981), and Nelson (1983), the channel has been interpreted as having bimodal structure leaving an "island" of undisturbed deposits. Channel activity affects the younger Pennsylvanian sediments and also the unconsolidated Pleistocene till. A limit to the eastern migration of channel development affecting the the Pennsylvanian sediments considered in this study can be identified by the abrupt change in event characteristics.

ACKNOWLEDGEMENTS

I would like to thank CONOCO, Inc., particularly and , for providing the field data and well information and from Consolidated Coal Inc. who also provided considerable well information. Thanks go to Chevron U.S.A. and Texaco for financial support.

Drs. Costain and Coruh have been extremely helpful during all aspects of this project. Dr. J. F. Read provided insight and very constructive comments concering the interpretation. Dr. E. S. Robinson has also provided constructive review of the writing. Thanks to all the graduate students and the staff of the Regional Geophysics Laboratory for all of the processing assistance and stimulating conversation during the course of my graduate studies.

Special thanks to the late whose interest, patience, and concern managed to keep financial considerations from interfering with the completion of this master's thesis.

Lastly, thanks to my family and my wife, , for their support, tolerance and perseverance.

TABLE OF CONTENTS

LIST OF ILLUSTRATIONS

LIST OF TABLES

BACKGROUND AND INTRODUCTION

High resolution seismic surveys require careful data acquisition. Frequency components must be recorded properly and preserved throughout data processing. Aspects of high frequency procedures are summarized by Sheriff and Geldart (1982,1983) and Neidell and Poggiaglioimi (1977).

Design of source and receiver arrays should emphasize signal recovery while sacrificing some benefits of noise attenuation. This is of particular importance when using band limited vibratory sources. Instrumentation must have adequate dynamic range to record both the signal and the noise simultaneously. If the signal-to-noise ratio (S/N) is good, source arrays may be eliminated entirely by processing each vibrator pad position as an individual source point (assuming vertical summing has not taken place in the field). Even with a poor S/N ratio, data quality may be improved by spectral whitening of individual sweeps before summing (Belcher, 1984).

Geophone arrays can be shortened to remove the low pass filter effect associated with low apparent velocities, particularly for shallow reflections. Arrays have been eliminated entirely in some circumstances to avoid phase distortion due to variations in coupling (Ziolkowski, 1977; Applegate and others, 1982). With proper design of field parameters, higher frequencies can be preserved optimizing temporal resolution.

Intrinsic damping and increased low frequency noise recorded because of priority placed on array design emphasize lower frequencies and reduce

resolution. Spectral whitening enhances high frequencies attenuated by intrinsic damping, especially in near surface layers where the quality factor, Q, can be as low as 25-95 (1.1-.29 dB/λ) (Angeleri and Loinger, 1984). Spectral whitening reduces the high energy, low frequency noise relative to the high frequency signal improving the S/N ratio.

Many conventional processing procedures act to filter high frequencies or otherwise reduce resolution. Applying dynamic (NMO) corrections to the data increases S/N but can discriminate against high frequency signal components. Selection of the proper mute is needed to avoid stacking stretched, far-offset traces. Proper selection of stacking velocities and static corrections are necessary to prevent further low pass filtering. Improper filter design over the bandwidth of the signal will effect wavelet shape and reduce resolution. Through proper processing, S/N ratio will increase and the signal bandwidth will be preserved allowing more exact waveform analysis and therefore a more detailed interpretation.

High resolution geophysical techniques, namely, single sweep geometry to reduce low pass filtering, Vibroseis whitening (Coruh and and Coruh, 1983), stretched automatic gain control (Coruh, 1985) to increase the S/N ratio and broaden the frequency bandwidth, as well as conventional processing methods have been applied to a seismic line which traverses shallow upper Pennsylvanian strata in the Illinois Basin.

The reflection from the Herrin No. 6 coal seam is of particular interest because of variations in the depositional history of both the coal and proximal strata. These variations have direct impact upon mining economies (Palmer and others, 1979) suggesting that high resolution re-

flection seismology could be of considerable economic importance where a detailed interpretation is obtained.

AREA OF STUDY

The study area is located in south central Illinois (Figure 1). A seismic line approximately 1.5 km long was acquired by Conoco, Inc., traversing Consolidated Coal Company properties in Montgomery County about 9 km east of Hillsboro, Illinois. The high resolution objectives are the Herrin No. 6 coal seam and overlying sediments which are interrupted by paleochannel development over the western third of the seismic line.

Figure 1. Location map showing seismic line: and mapped paleochannel interruptions of the Herrin #6 coal seam; Walshville channel contemporaneous, Anvil Rock channel erosional. (Modified from Nelson, 1983).

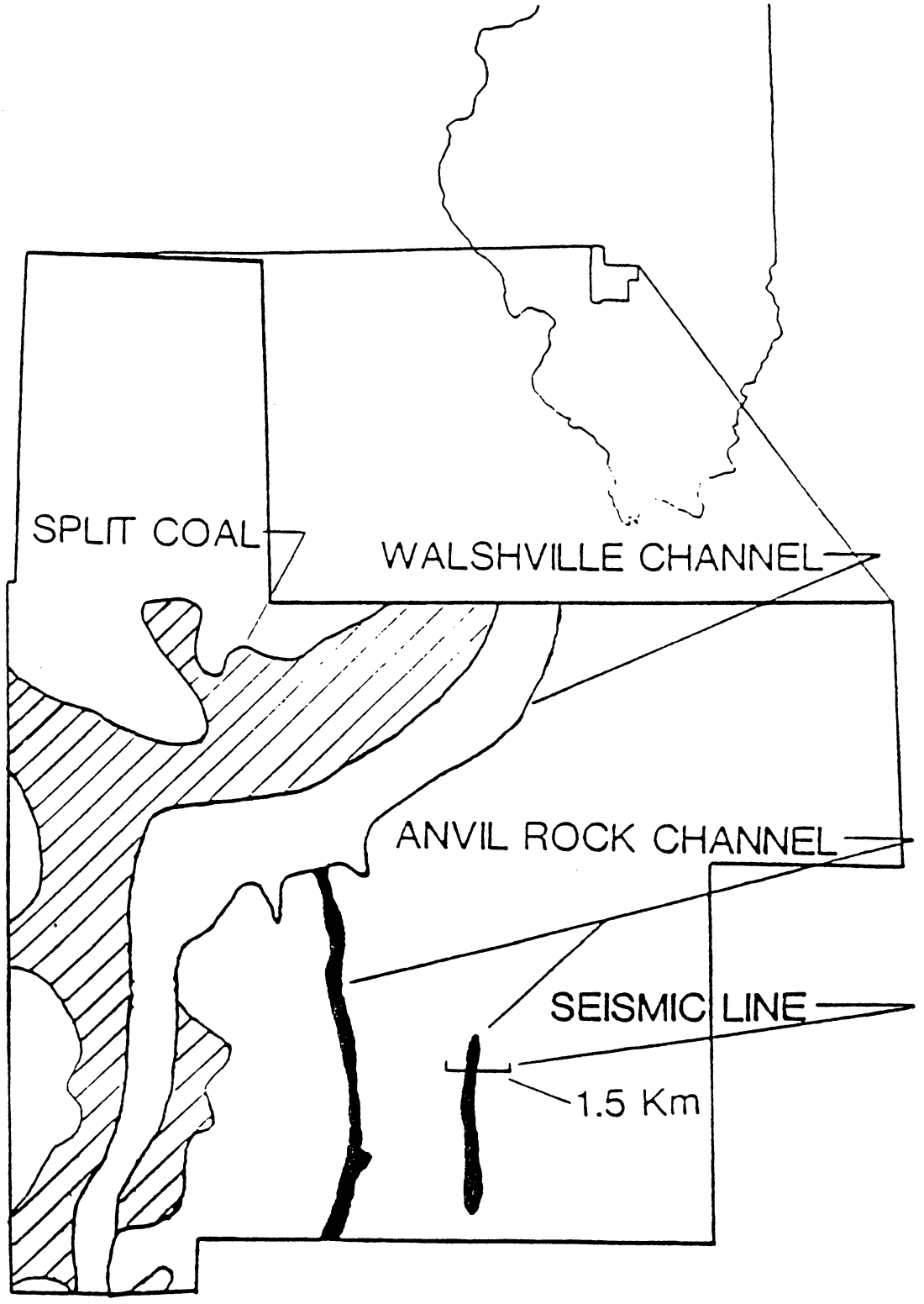

MONTGOMERY COUNTY, ILLINOIS

DEPOSITIONAL ENVIRONMENT

The sedimentary rocks in the area were deposited on the western shelf of the Illinois Basin. Seventeen deltaic cycles involving upper and middle Pennsylvanian sediments have been identified by Wanless and others, 1970. The delta complex upon which the peat forming the Herrin #6 seam accumulated forms its apex to the north and east of the study area in central Indiana. The principal distributary channel system is directed to the south and the southwest (Figure 2a).

The formation of the Herrin coal follows a marine regression depositing the peat directly over marine muds (Wanless and others, 1969). As sea level fell and the delta advanced, peat accumulation near the delta apex was restricted to thin deposits. Maximum accumulation took place along the arcuate front of the continually exposed prodelta. The thickness of the Herrin coal is shown in Figure 2b.

The drowning of the peat-forming sequence was marked by the deposition of a black, carbonaceous shale (Anna Shale Member) laid down in brackish water or logoonal conditions (Palmer and others, 1979). The Anna Shale Member directly overlies the Herrin coal except in areas influenced by channel development (Nelson, 1983). Both contemporaneous and post-depositional channel fills (see Figure 1) produced overbank or splay deposits of deltaic gray shale. These deposits may either directly overly the Herrin seam or influence the lithologic sequences above the coal.

Figure 2. Deltaic complex(a) and thickness(b) of Herrin coal: Thickest deposits found along the delta margin. Paleocurrent direction is south to southeast. (Modified from Wanless (1970)(a) and Willman (1975)(b)).

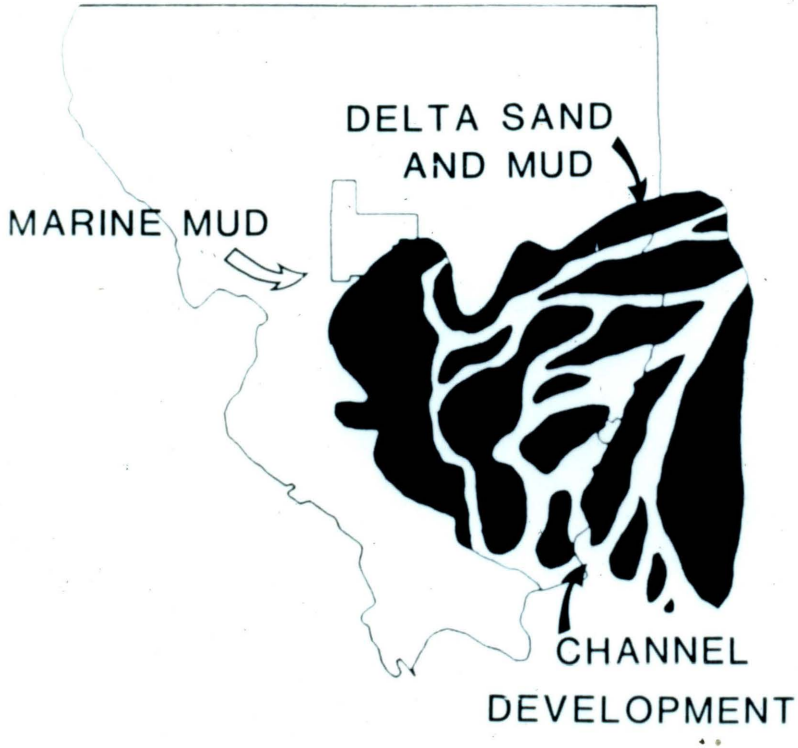
DELTA SAND
AND MUD
MARINE MUD
CHANNEL
DEVELOPMENT

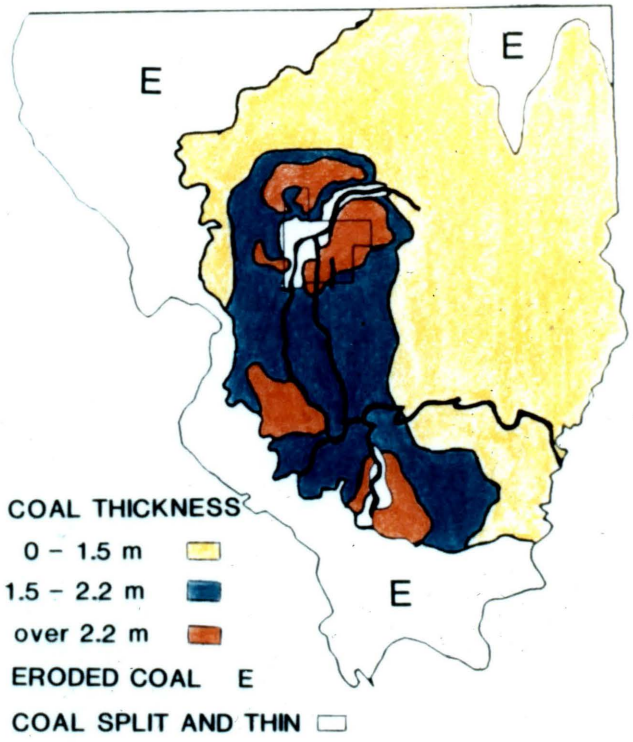
E
E
E
COAL THICKNESS
0 – 1.5 m
1.5 – 2.2 m
over 2.2 m
ERODED COAL E
COAL SPLIT AND THIN

GEOLOGIC SETTING

A generalized lithostratigraphic sequence for the study area is given in Figure 3. The Herrin No. 6 coal member and associated sediments of the Carbondale Formation are upper Pennsylvanian in age. The Herrin seam is the major economic coal of the area, varying in thickness from 2-3 m. Other seams in the formation include the underlying Springfield No. 5 seam and the overlying Danville No. 7 seam. Both of these coals are thin (0 to 1 meter) in the area and may become laterally discontinuous (Hopkins and others, 1979).

Gray deltaic shales are the most prominent lithology in the Carbondale Formation. Black, marine shales and limestones are present as thin but laterally continuous deposits. Sandstones commonly occur as channel facies of up to 30 m in thickness. Both the gray shales and sandstones change rapidly in thickness (Nelson, 1979).

The overlying Pennsylvanian Modesto and Bond Formations maintain the same general character. Gray shales predominate and several members are laterally persistent. The sandstones and gray shales continue to vary in thickness. The coals, however, become thinner and the marine shales and limestones thicken as the sediments get younger (Willman and others, 1975). Pleistocene glacial till and loess directly overlie the Bond Formation in erosional contact. The glacial deposits are about 15-30 m thick with local accumulations of up to 50 m.

Figure 3. Generalized lithostratigraphic sequence: Showing upper Pennsylvanian strata from horizon of Herrin coal seam to the Pleistocene-Pennsylvanian unconformity. Note the thin but normally continuous marine deposits, presense of channel activity throughout the section, and the complex relationship between the Herrin coal and the overlying sediments.

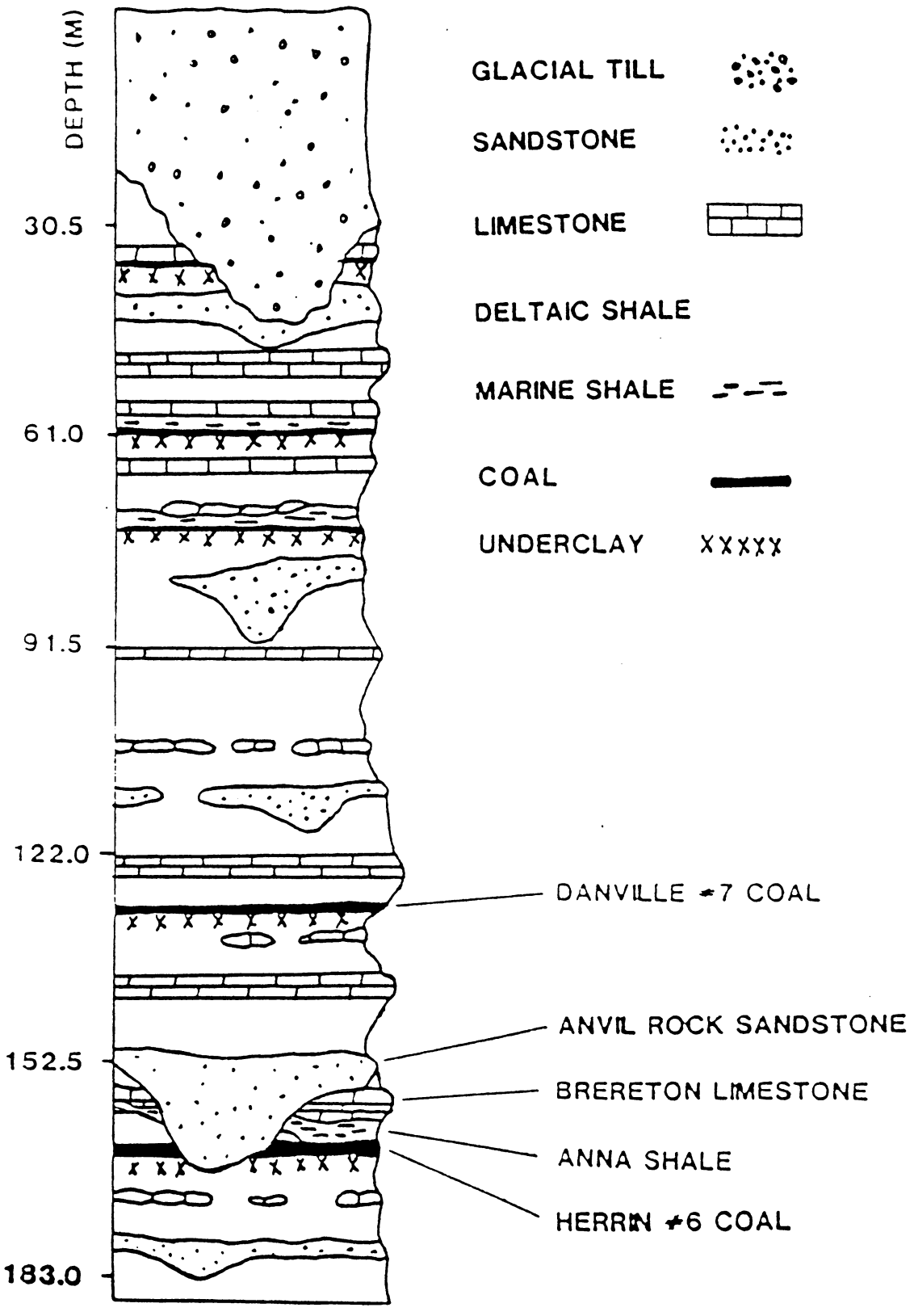
DEPTH (M)
30.5
61.0
91.5
122.0
152.5
183.0
GLACIAL TILL
SANDSTONE
LIMESTONE
DELTAIC SHALE
MARINE SHALE
COAL
UNDERCLAY
DANVILLE #7 COAL
ANVIL ROCK SANDSTONE
BRERETON LIMESTONE
ANNA SHALE
HERRIN #6 COAL

In the study area, marine deposits (Anna Shale Member and Brereton Limestone Member) directly overlies Herrin coal. The underclay is very well developed and has marine mud origins. The Herrin coal where overlain by the marine sequence tends to be of uniform thickness with some variability near channel fills. Where channels erode into the Herrin coal the contact may be a sharp, high angle or gradational boundary.

Sandstone thicknesses of greater than 7 m probably represent channel facies which interrupt the lateral continuity of the depositional sequences (Potter and Simon, 1961). In some instances, younger channel sandstones are juxtaposed against underlying channel facies developing thicker sandstone accumulations (Anderson, 1963). The Anvil Rock Sandstone Member fills a channel which has completely eroded through the #6 seam and many overlying members. The channel deposits are variable, typically containing shale, siltstone, and coal as well as sandstone (Potter and Simon, 1961). A contemporaneous paleochannel lies to the west of the study area (Figure 1), renamed the Walshville Channel after first being identified as the Anvil Rock Sandstone by Potter and Simon (Palmer and others, 1979). The voluminous channel (2-9 km wide) has affected the lateral continuity of the Herrin coal and associated lithologies with discontinuous gray shale splay deposits (Nelson, 1983).

DATA

FIELD GEOMETRY MODIFICATIONS

Conoco, Inc. acquired the seismic data using an energy weighted (2:1 ratio) nonlinear, 2-element source array and a linear 20-element receiver array (Chapman, Brown, and Fair, 1981. and Chapman, personal comm., 1984). The recording parameters are listed in Table 1. The data were recorded using a Geosource MVS-9 system.

Field acquisition procedures which involve multiple vibrator points with common receiver positions conventionally sum contributions from the vibrator points to form a single source point located by the midpoint of the array. Single sweep acquisition considers each vibrator point as a source point during subsequent processing. Instead of using single-element energy sources, original processing involved ten 2-element common receiver source arrays which were summed to obtain a 20-element source array. Following the single sweep processing concept described by Belcher (1984), this study considers each 2-element source array individually. Low pass filtering of high frequencies in the signal bandwidth were reduced by using the modified source array, sacrificing noise attenuation (Appendix A).

Geometry modifications are needed to compensate for the incremental advance in source point location without a corresponding roll-up of receiver groups. This modification is periodic; common receiver groups remain fixed for the number of concurrent sweeps forming the original source

array. Digicon DISCO software has flexible geometry routines which make this modification straightforward. Spread geometry for twenty contiguous 2-element source arrays is shown in Figure 4.

Because of the energy level differences between the vibrators forming the 2-element source array, resulting source point locations are weighted rather than defined by the array midpoint. The weighted source point locations are influenced by the energy level differences between vibrators and the change in travel time as the distance between the source array and the geophone spread change.

Source locations have been identified by travel time analysis. Normal moveout corrections are applied and traces stacked for a group of common receiver source arrays. The source point location is varied until horizontal reflections flatten. If the source points are located incorrectly, false dip appears on the stacked section in increments of the common receiver array length. The resulting "piggy-back" appearance of the near surface reflectors is shown in Figure 5where normal moveout corrections are more sensitive to time-distance errors.

Reprocessing of the field data was done using the facilities of the Regional Geophysics Laboratory at Virginia Tech utilizing a VAX 11/780 computer with Digicon DISCO software. The processing parameters are summarized in Table 2.

Figure 4. Spread geometry displaying 2-element source array modifications.: Note the variation in 2-element source array length which changes the response characteristics for the array, and the overlap in shot point locations causing fold coverage to be variable.

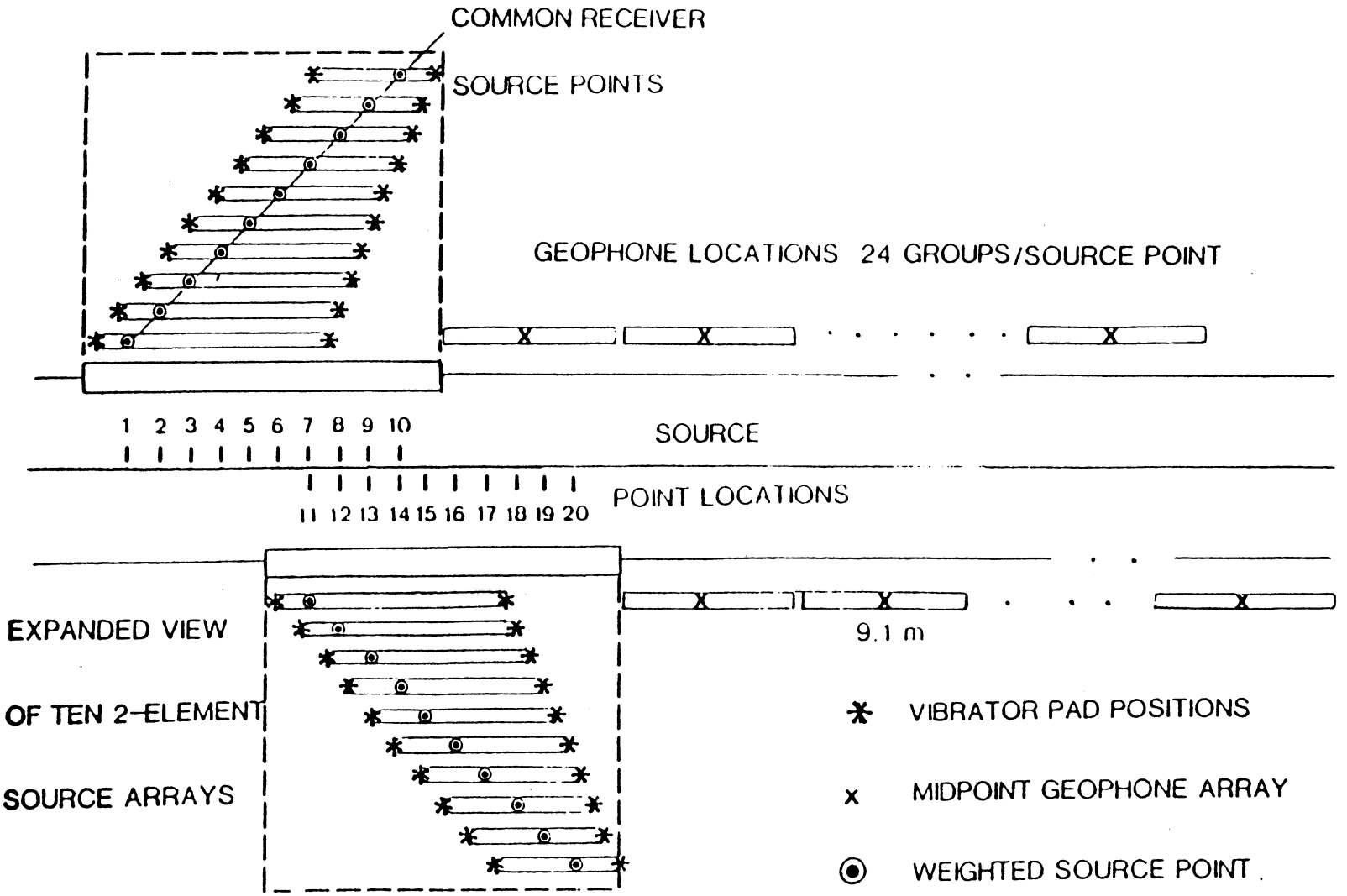
COMMON RECEIVER
SOURCE POINTS
GEOPHONE LOCATIONS 24 GROUPS/SOURCE POINT
1 2 3 4 5 6 7 8 9 10
SOURCE
11 12 13 14 15 16 17 18 19 20
POINT LOCATIONS
EXPANDED VIEW
OF TEN 2-ELEMENT
SOURCE ARRAYS
9.1 m
VIBRATOR PAD POSITIONS
MIDPOINT GEOPHONE ARRAY
WEIGHTED SOURCE POINT

Figure 5. Error in spread geometry causing apparent dip in shallow section.: The error is apparent in the section from 60 to 100 msec.

0.1
SEC
0.2
0.1
SEC
0.2

Table 1. Recording Parameters

A	B
Record Time (sec)	16
Sweep Length (sec)	15
Sample rate (msec)	1
Spread Geometry (m)	End On 0 - 14(avg) - 235
Fold	12-24 (34 max)
Receiver Group Spacing (m)	9.1
Receiver Element Spacing (m)	0.5
Receiver Element Weighting	Linear (24 groups/sp)
No. of Vibrators; Weighting	2; Energy Weighted 2:1
Source Element Spacing (m)	Variable; 6.4-12.5
Sweep Frequency Band (Hz)	260-50
Sweep Taper (msec)	200

Table 2. Data Processing Sequence

NUMBER	PROCESSING STEP
1.	Demultiplex
2.	VSW; AGC (100 msec window), Correlation
3.	SAGC; 5 sec stretching function, 50 msec AGC
4.	Edit
5.	CDP Sort
6.	Filter; Wavelet shaping filter
7.	Residual Statics (3 passes)
8.	NMO (15 velocity functions - Appendix B)
9.	Mute
10.	Filter Low Pass filter (0-100 msec)
11.	Stack (maximum 34 fold)
12.	Migration 3 msec/CDP dip

SIGNAL PROCESSING

S/N RATIO AND SPECTRAL BANDWIDTH

Improvements in S/N ratio were accomplished by Vibroseis whitening (VSW) (Coruh and Costain, 1981). An AGC window of 100 msec was used. Further spectral whitening was accomplished using stretched automatic gain control (SAGC) (Coruh, 1985). A 5 sec stretching function, frequency range 50-270 Hz, and a 50 msec AGC window was used.

Amplitude spectra of shot data without whitening, and with both VSW and SAGC, applied are shown in Figure 6a. The Overall S/N ratio is improved after whitening. The 85 Hz noise apparent before whitening is reduced to the amplitude level of the signal. This narrow band may be noise not attenuated by the field recording array (Appendix B).

Spectral bandwidth is increased after each whitening process. Improvement in high frequency whitening using SAGC after VSW may be attributed to the use of synthetic sweep traces in the SAGC process rather than an estimation of the sweep traces in VSW which may become more unstable at high frequencies due to baseplate decoupling (Hoover and others, 1984).

Spectral balance is also evident from inspection of the autocorrelation of common shot data before and after whitening (Figure 6b and Figure 6c). The autocorrelation of the whitened data trace (c) is almost identical to the Klauder wavelet (d) for a time of 12 msec measured from zero lag. Note the absence of reverberations from (c) which dominate (b).

Figure 6. Spectral improvements from whitening.: (a) compares amplitude spectra before(heavy) and after(light) whitenig is applied. Note enhancement of high frequencies and reduction of the energy spike at 85-120 Hz. (b) and (c) are corresponding autocorrelation functions; note similarity between (c) and the Klauder wavelet (d).

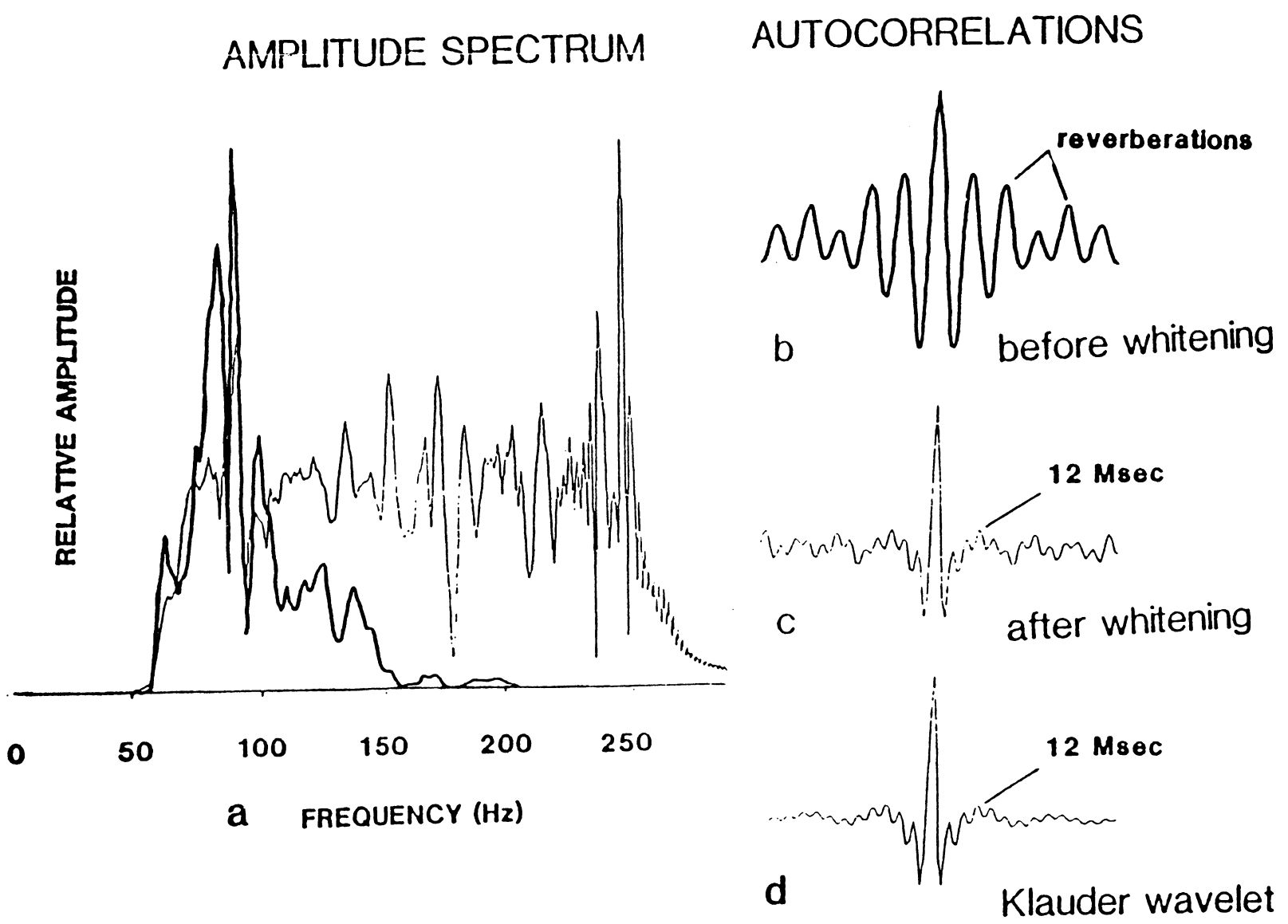
AMPLITUDE SPECTRUM
RELATIVE AMPLITUDE
0
50
100
150
200
250
a
FREQUENCY (Hz)
AUTOCORRELATIONS
reverberations
b
before whitening
12 Msec
c
after whitening
12 Msec
d
Klauder wavelet

FILTERING AND WAVELET PROCESSING

Wavelet shape governs the resolution potentially derivable from seismic data. Zero-phase wavelets have been shown to exhibit minimum length properties and provide the best resolution when compared with non-zero phase wavelets having the same amplitude spectrum (Schoenberger, 1974). Spectral shape, which affects temporal characteristics, namely, main lobe to side lobe amplitude ratio, main lobe width and side lobe length, must be considered for optimum resolution (e.g., Koefoed, 1981). Zero-phase filters can be designed to obtain the desired temporal character.

For reflections from thin layer strata with high acoustic impedance, the Klauder wavelet (Figure 6d) and the pre-stack autocorrelation function (Figure 6c) do not provide optimum resolution (Berkhout, 1984). An optimum window function described by Berkhout, 1984, defines a filter that minimizes signal length. The filter is given by;

$$A(f) = \cos\{\pi/2(f-f_c)\}/\Delta f \quad \text{for } f_1 < f < f_h$$

and is zero for all other frequencies.

Where;

$$f_c = 0.5*(f_h + f_1) = (250 + 50) = 150 \text{ Hz.}$$

and,

$$\Delta f = 0.5*(f_h - f_l) = (250 - 50) = 100 \text{ Hz}.$$

The amplitude spectrum and the waveform of a Klauder wavelet before and after filtering are shown in Figure 7. Side lobe energy resulting from the steeply sloped amplitude spectrum of the Klauder wavelet is greatly reduced with minimal increase in the main lobe/side lobe ratio after filtering.

Wavelet processing of land data involves difficult statistical methods of deconvolution in order to arrive at an interpretable waveform. Spectral whitening techniques applied in the early stages of this study produced a 'deconvolution-like' effect by flattening the spectral bandwidth (Hoover and others, 1984). Because the filter applied to the data is designed to optimize wavelet time domain characteristics, the result is an interpretable waveform which has been obtained in a simple, straightforward manner. Conventional gapped (or spike) deconvolution has been avoided after testing has shown negative results on the data. Thus, phase distortions associated with deconvolving zero-phase Vibroseis data have not been introduced (Gibson and Larner, 1984).

VELOCITY ANALYSIS AND STATICS

Lateral variations in the near surface have made it necessary to make frequent determinations of stacking velocities. The stacking velocities were evaluated every 100 CDP's (76 m) where reflectors are influenced by

Figure 7. Optimizing filter applied to Klauder wavelet: Amplitude spectra and waveform before and after filter application. Note loss of side lode energy after filtering.

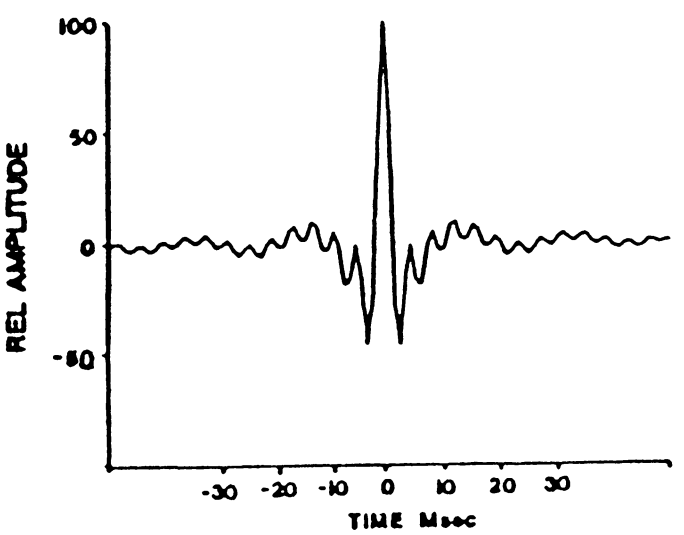
100
50
0
-50
REL AMPLITUDE
-30 -20 -10 0 10 20 30
TIME Msec

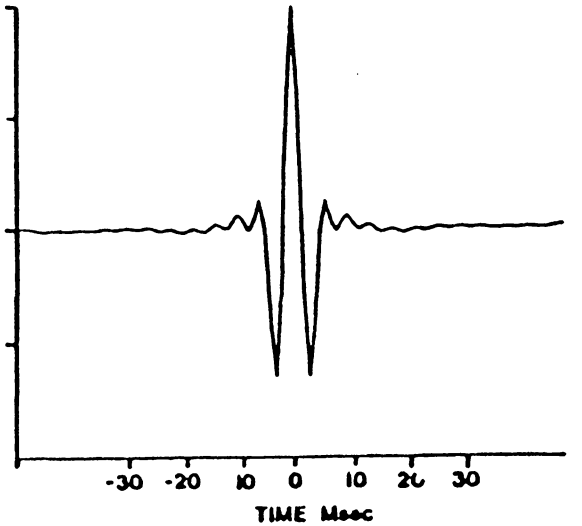
-30 -20 10 0 10 20 30
TIME Msec

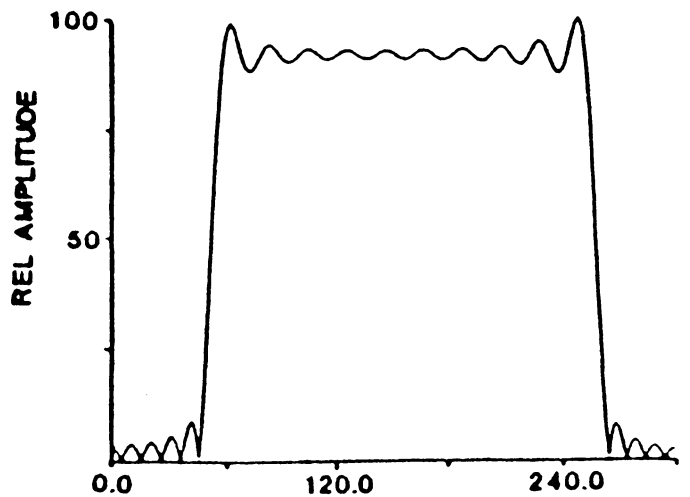
100
50
REL AMPLITUDE
0.0
120.0
240.0

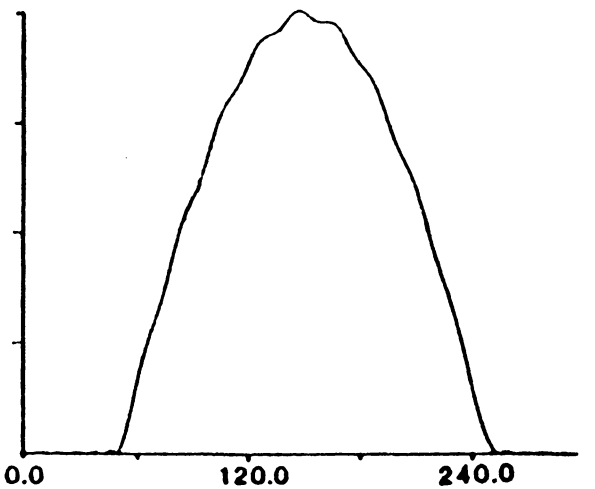
0.0
120.0
240.0

channel activity (CDP 100-1100) and every 200 CDP's (152 m) for the remainder of the seismic line. Rapid changes in layer thickness also caused static shifts which led to an iterative procedure for establishing the appropriate velocity function. The final velocity function is given in Appendix B.

A common problem encountered while processing land data is static shifts within a CDP gather. If the static shift is left uncorrected, the stacked CDP data will be filtered; high frequencies present in the individual traces will be attenuated by the stacking process. In Figure 8, two 150 Hz Ricker wavelets are summed with increasing amounts of static shift. Note the amount of high frequency attenuation with an error of 3 msec (3 sampling intervals). The attenuation is severe because the period of the static error approaches the predominant period of the Ricker wavelet.

Residual statics problems are accentuated when wavefronts encounter zones of highly variable velocity and thickness, e.g., sediments disturbed by channel development. Low pass filtering was applied to the data affected by what has been interpreted as channel development before the static shifts were determined minimizing problems with cycle skips.

Datum statics were not necessary in processing the seismic data because of low topographic relief and poor identification of first breaks in the shot data. Three residual static computations were made, one of which specifically addressed the low frequency events in the channel area. A stacked section before application of static corrections is shown in Figure 9a. Figure 9b shows the section after residual statics are applied. Compare, especially, the improvement in events occurring before

Figure 8. Frequency loss caused by static errors.: Two Ricker wavelets summed with varying amounts of static error.

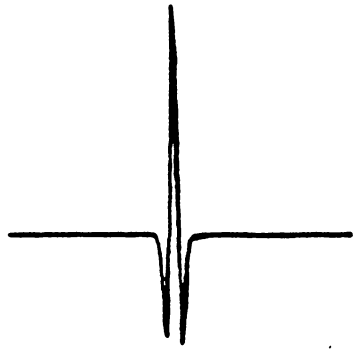

NO STATIC ERROR

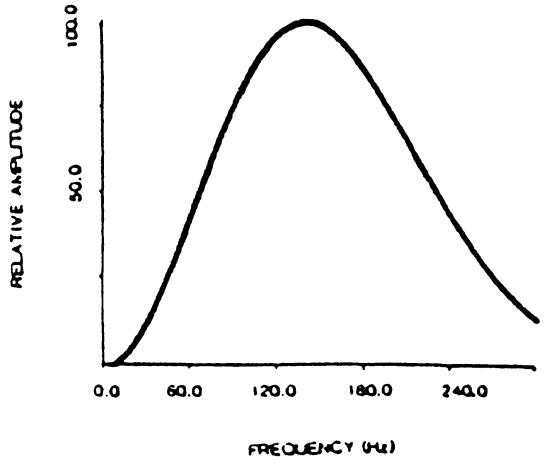

2 MSEC STATIC ERROR

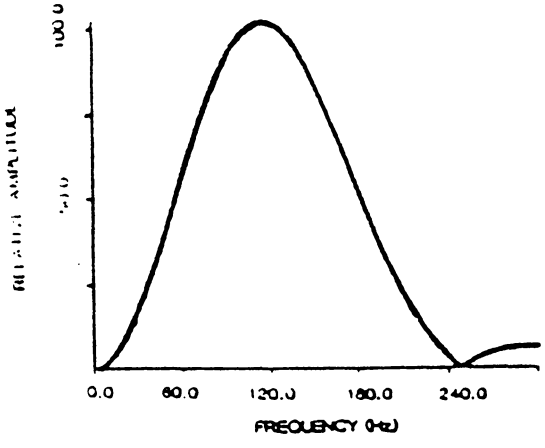

3 MSEC STATIC ERROR

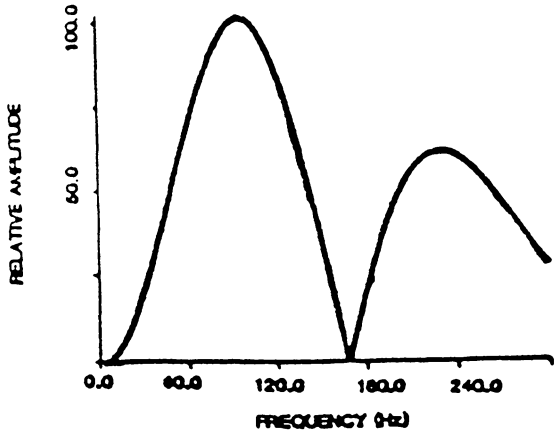

150 Hz RICKER WAVELET

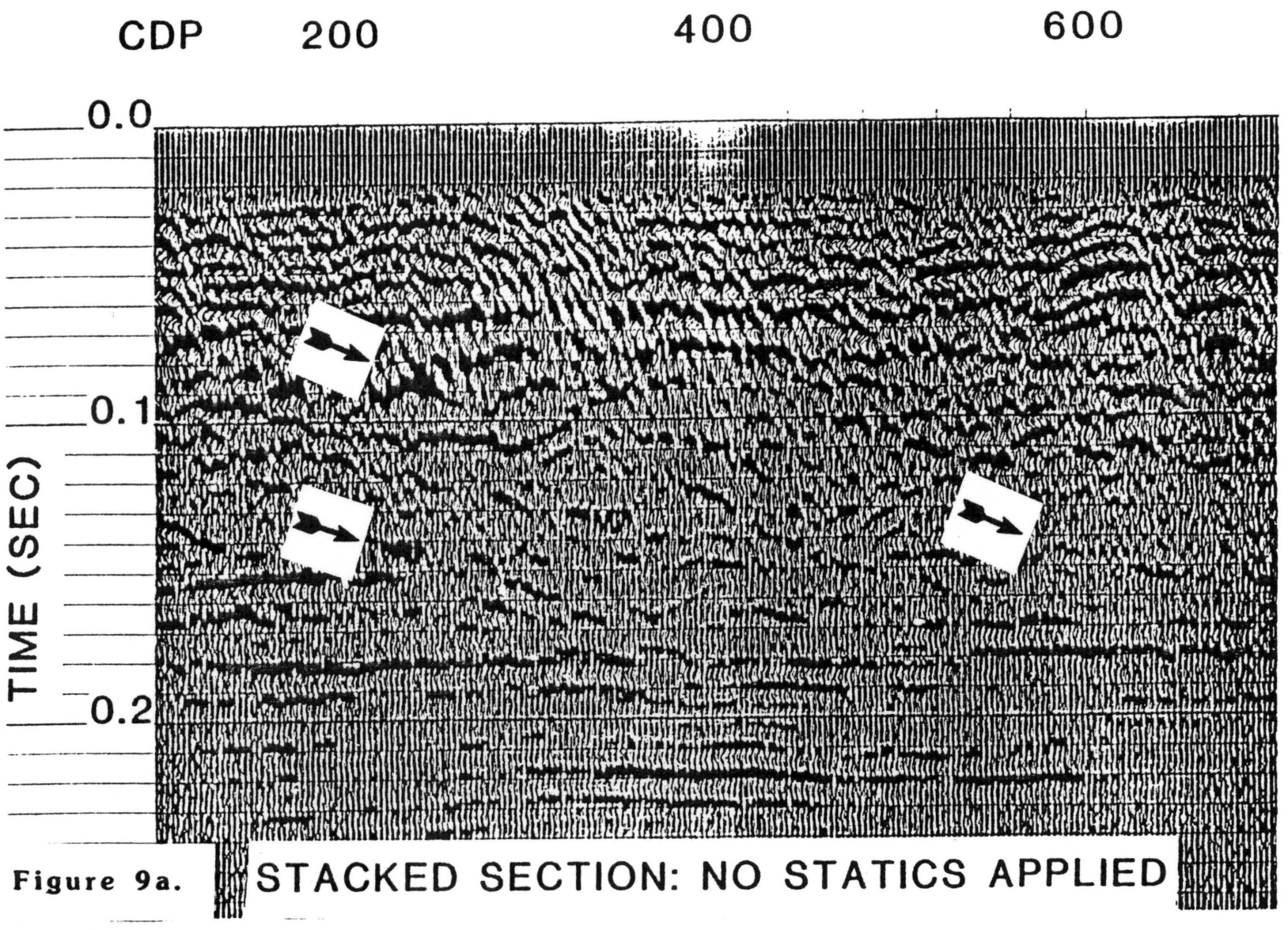
CDP
200
400
600
0.0
0.1
0.2
TIME (SEC)
STACKED SECTION: NO STATICS APPLIED

Figure 9a.

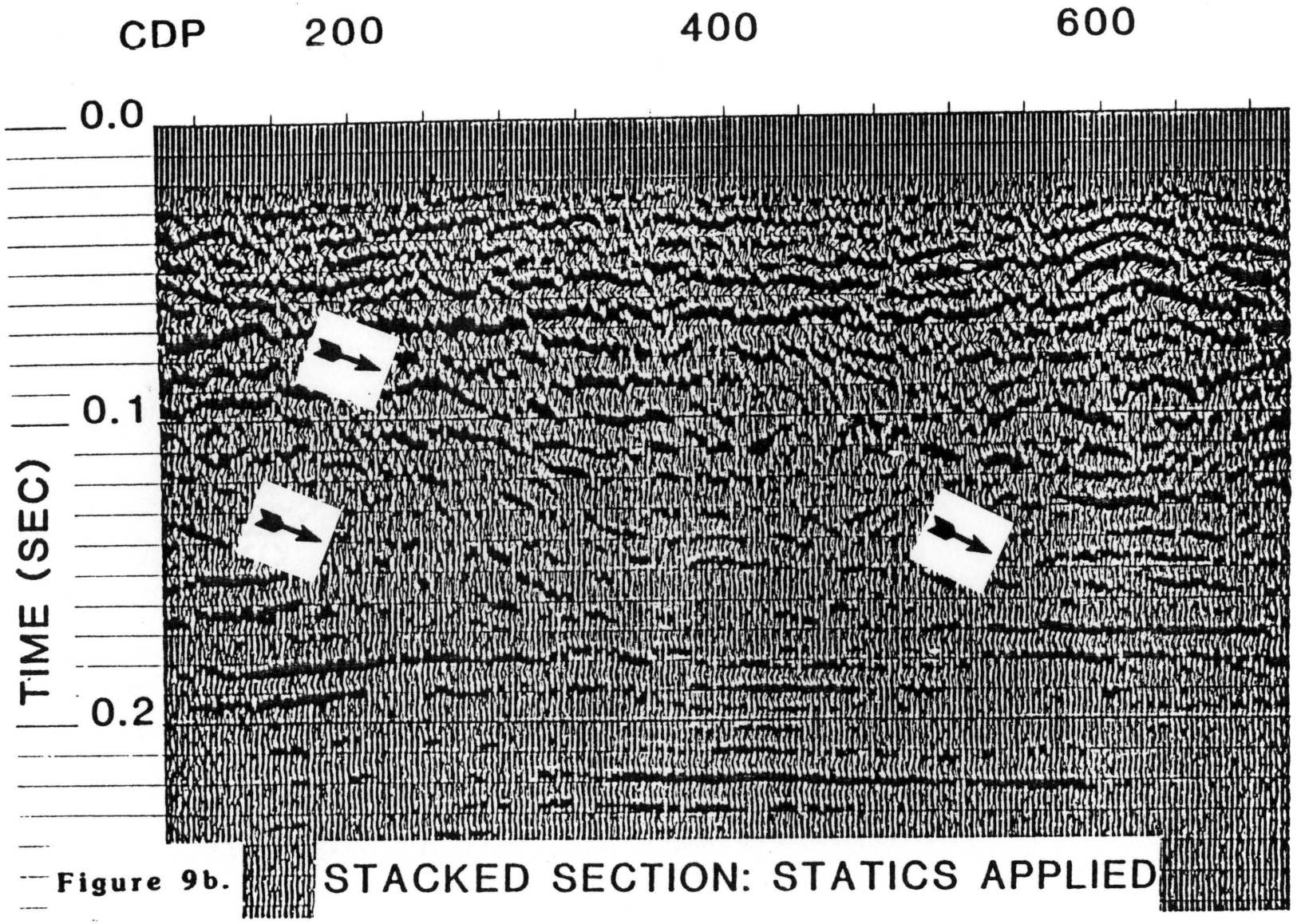
CDP
200
400
600
0.0
0.1
0.2
TIME (SEC)
STACKED SECTION: STATICS APPLIED

Figure 9b.

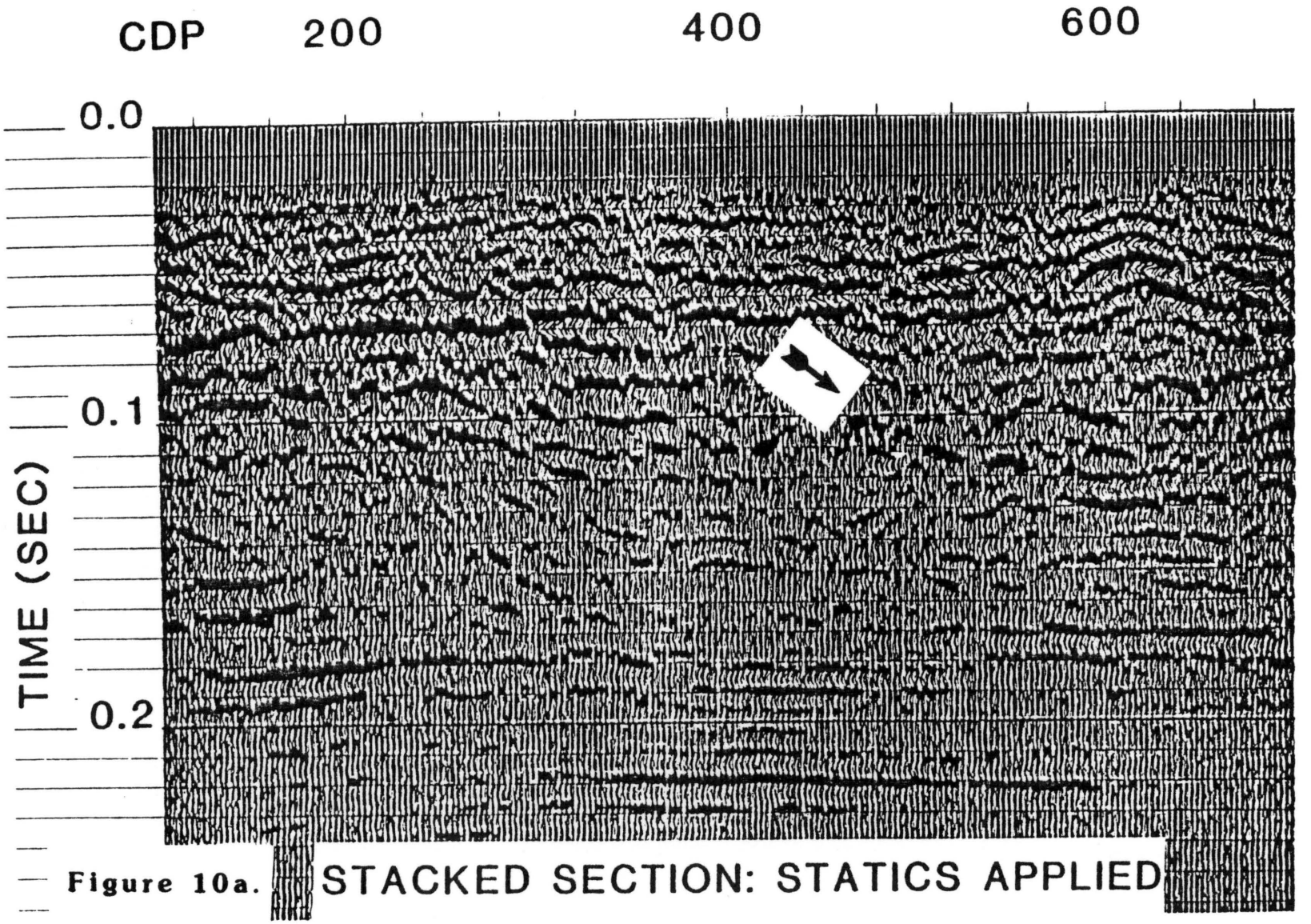
CDP
200
400
600
0.0
0.1
0.2
TIME (SEC)
STACKED SECTION: STATICS APPLIED

Figure 10a.

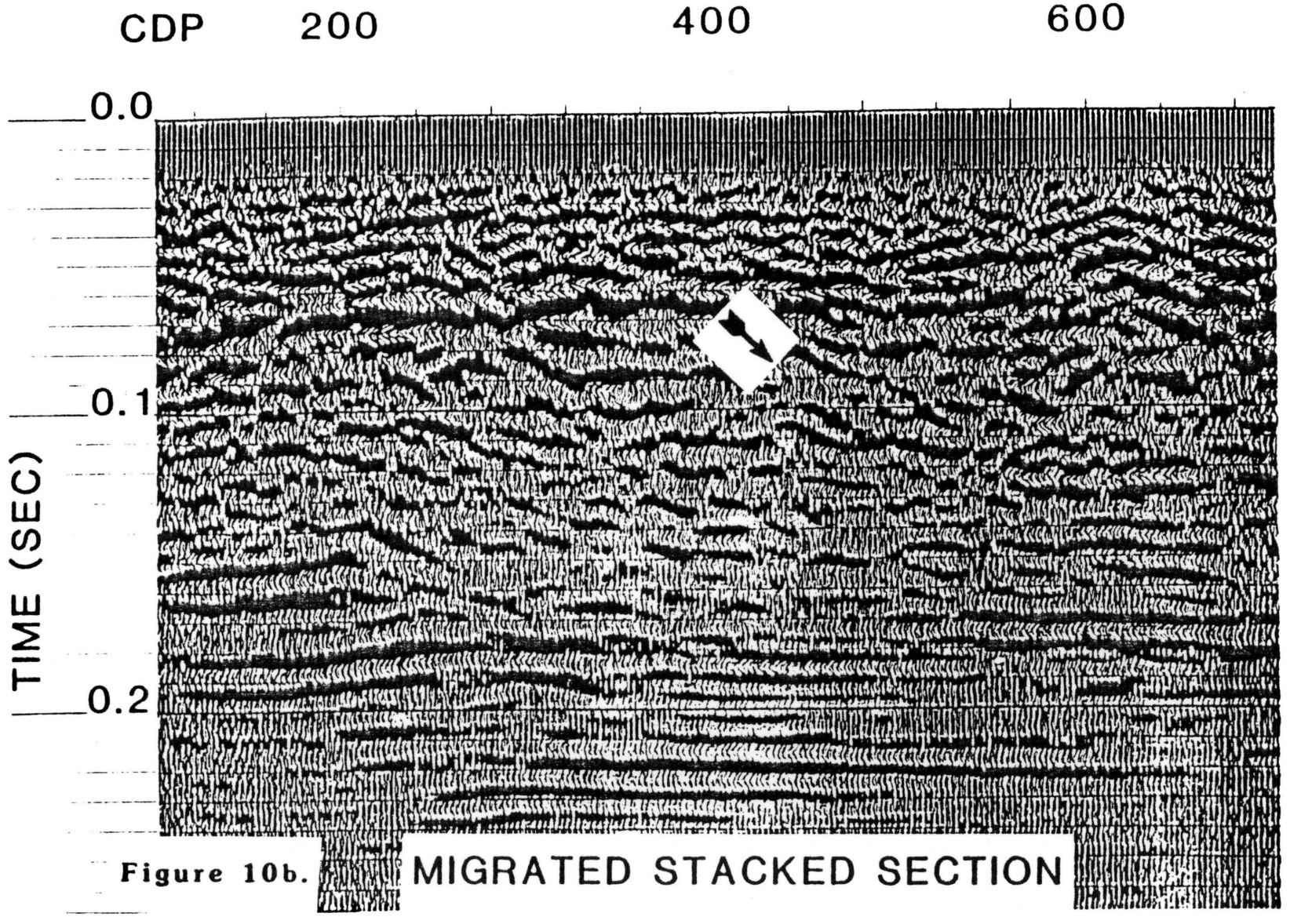

Figure 10b.

100 msec and the increase in frequency content and coherency of reflectors indicated by arrows.

Wave equation migration was applied to the stacked data. Although the events are primarily flat lying, migration procedures were found effective in improving data quality (Figure 10). Diffracted events, especially in the region of channel development (shown by arrows), were reduced making primary events more identifiable. The final migrated stacked section is shown in Figure 11 (in Pocket).

In Pocket.

Figure 11. Final migrated stacked section.: Herrin coal complex is shown as event 'H' and the arrow defines the position of the top of the seam in the complex.

WAVEFORM ANALYSIS AND INTERPRETATION

WAVEFORM ANALYSIS; HERRIN COAL COMPLEX

Examination of the final migrated section (Figure 11) shows a uniform high amplitude, designated H, at 150 msec. This event is correlated with the Herrin #6 coal seam. This is verified with drill hole information from hole HB-87 located near CDP 1090 (Appendix C). The waveform associated with the Herrin seam is from a complex of horizons above and below the coal. A simplified stratigraphic column for HB-87 is shown in Figure 12b. The overlying black shale and limestone are correlated with the Anna shale member and the Brereton limestone member. A synthetic seismogram developed from the hole information is shown in Figure 13. The synthetic seismogram was formed by convolving a 50-260 Hz Klauder wavelet with the spike series. The trace was then filtered with the waveshaping filter described previously. Further low pass filtering was necessary to match amplitude spectra of the synthetic and the real stacked data.

The synthetic is compared directly with the migrated section. There is very good correlation between waveforms associated with the Herrin coal complex (150 msec), the Pleistocene till-limestone contact (55 msec), and the limestone sequence above the Herrin coal complex (120 msec). Time differences between events do not match exactly because interval velocities are approximated from stacking velocities (Appendix B) and velocity values given by Waters (1981).

Figure 12. Stratigraphic column for hole HB-87 (CDP 1090).

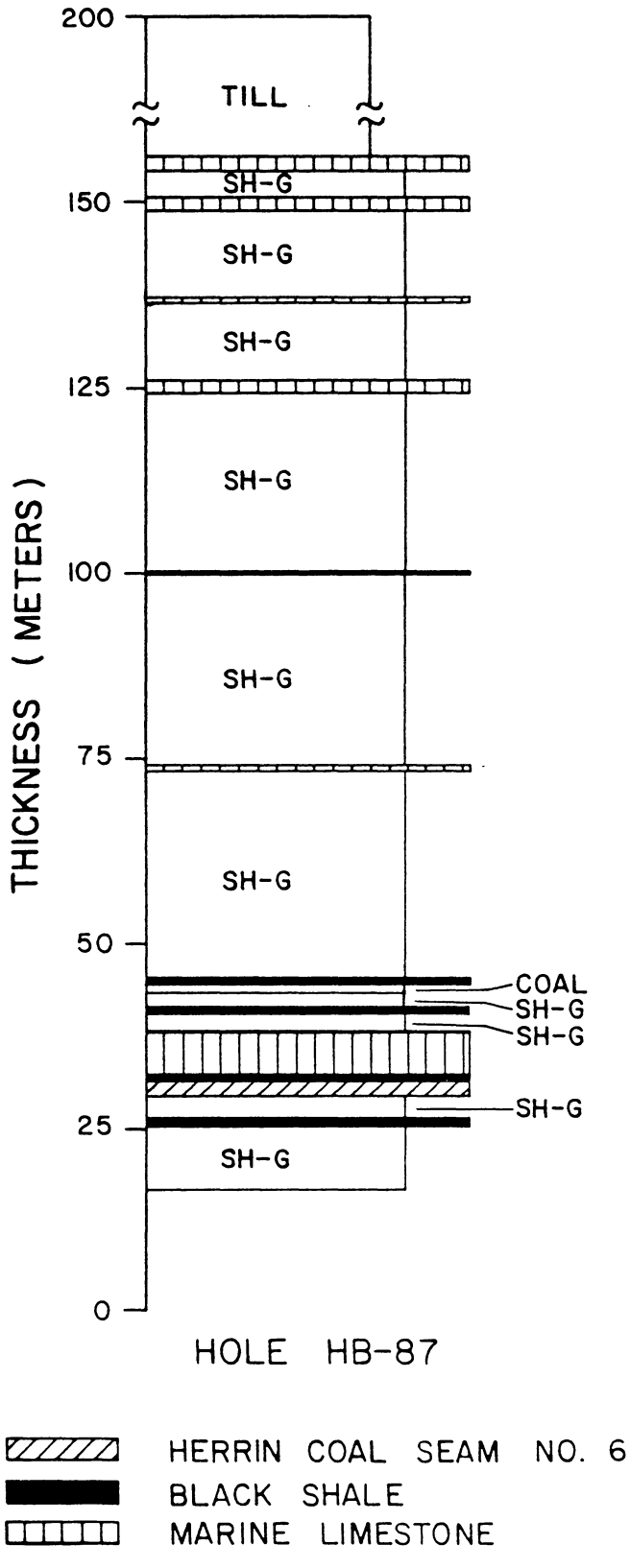
200
150
125
100
75
50
25
0
THICKNESS (METERS)
TILL
SH-G
SH-G
SH-G
SH-G
SH-G
SH-G
SH-G
COAL
SH-G
SH-G
SH-G
SH-G
HOLE HB-87
HERRIN COAL SEAM NO. 6
BLACK SHALE
MARINE LIMESTONE

Figure 13. Synthetic seismogram for hole HB-87: Compared with the migrated stacked section. Note good agreement in waveform character, timing differences due to lack of velocity control.

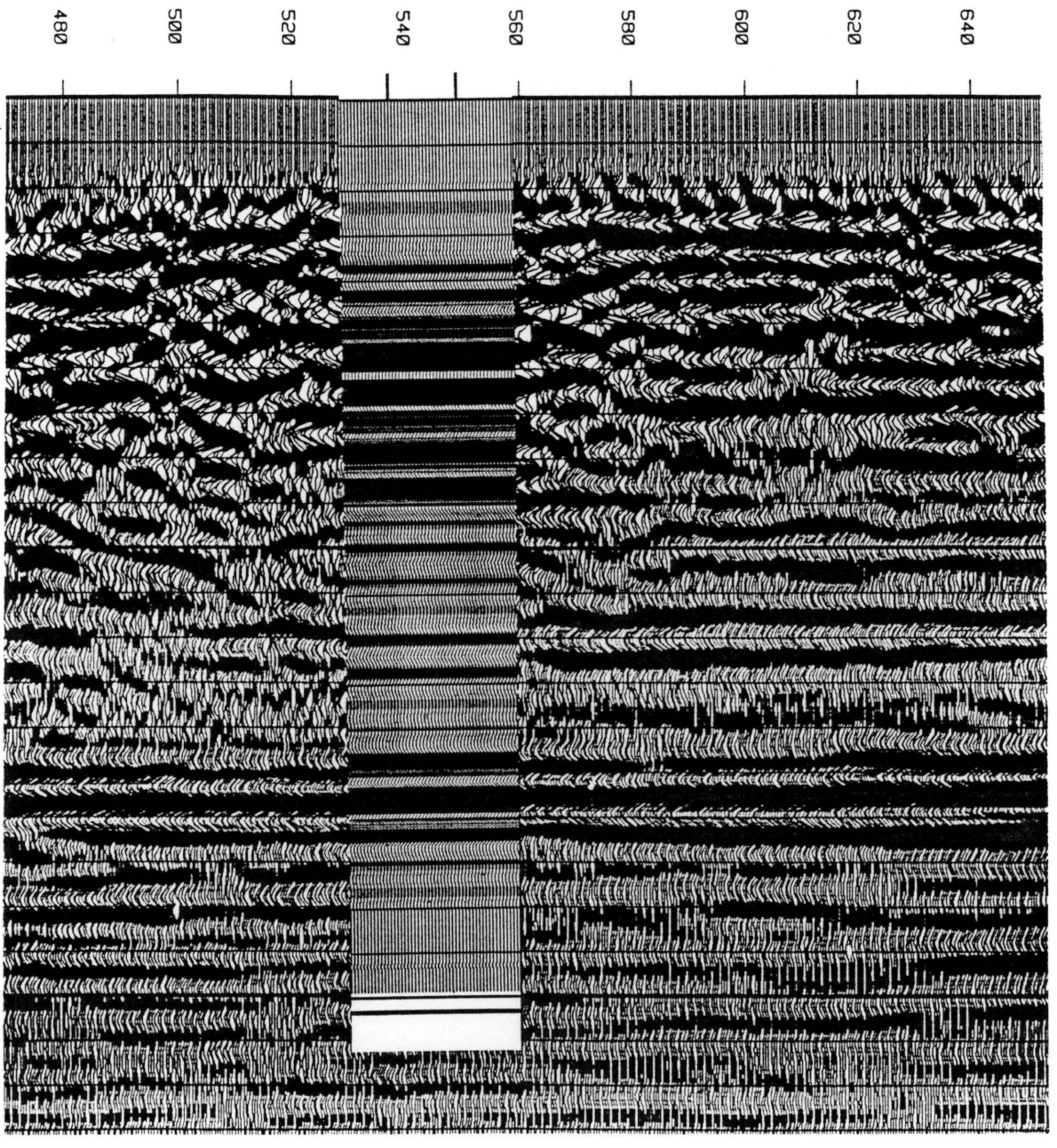

Figure 13. Synthetic seismogram for hole HB-87.

The close correlation in waveform character between the synthetic and the real migrated stacked section allows confident interpretation of the strong reflections associated with the Herrin coal, the thin limestone events, and the Pleistocene unconformity. Lack of good velocity control, however, has limited the effectiveness of modeling more complex geology such as the areas involving channel development.

INTERPRETATION

An interpreted seismic section is shown in Figure 14 (in pocket). The uniform high amplitude reflection at 150 msec (shown in red) is interpreted to be the Herrin coal complex. The coal seam itself is identified by the upper inflection point associated with the middle negative peak (shown by the arrow in Figure 11). Test hole information (Appendix C) shows that the complex of events surrounding the Herrin coal seam change laterally. Thus, variations in the upper and lower negative peaks can be correlated with lateral changes in thickness of surrounding units, e.g., marine shale and the gray deltaic shale. From hole information, apparent dip of the Herrin coal complex from east to west shown on the interpreted section is real but exaggerated by velocity pull-up associated with the eastward thinning of the Pleistocene glacial till (boundary shown in orange). Approximately 3 msec of the 9 msec apparent dip can be correlated with the 4 m decrease in depth of the Herrin coal seam.

Four uniform reflectors which appear higher in section (55, 65, 100, 120 msec) are interpreted to be marine transgressive sequences predominately limestone with possible black shale. The marine events are

In Pocket.

Figure 14. Interpreted seismic section.: Data acquired by Conoco Inc. and reprocessed and interpreted by Regional Geophysics Laboratory, Virginia Tech (1985).

colored dark blue. The waveform identifying the marine sequences are low amplitude events typical of thin bed response with thickness below tuning. This correlates with test hole data which identifies the marine sequences as thin (less than 3 m usually) units imbedded in thick units of deltaic shale. The two marine sequences at 55 and 65 msec are interpreted as two limestone layers separated by an eastward thickening deposit of deltaic sediments.

Deltaic sequences involving shale (light blue) and sand (yellow) separate the marine events. The sand appears as possible overbank deposits (at 135 msec) from CDP 1200 to 2000 and (110 msec) from CDP 1400 to 1900. Minor abandoned channel fills are interpreted near the eastern edge of the seismic line labelled C (110 msec, CDP 1800 and 135 msec, CDP 1860). Shale and silt replace the uniform sand in the channel fill reducing the amplitude contrast between the otherwise sandy horizon and the surrounding shale. Depressions in the overlying marine sequences signify differential compaction and identify the abandoned fills. Over the western half of the section (CDP 100-1100), the sand becomes channel phase and erodes into the underlying events including the Herrin coal complex. Bimodal channel development is apparent with an "island" of undisturbed horizons centered at CDP 600. Events from the marine sequence at 120 msec through the event marking the bottom of the Herrin coal complex at 172 msec can be matched exactly with undisturbed horizons to the east (e.g., CDP 1200). A detailed comparison is shown in Figure 15.

The marine sequence at 120 msec identifies the end of the regressive period during which major channel activity took place in the study area. The marine event has apparent structure over the channel development

Figure 15. Comparison of undisturbed horizons with "island".: Note correlation of waveform from 120 msec to 170 msec.


0.1
0.1
SEC
SEC
0.2
0.2

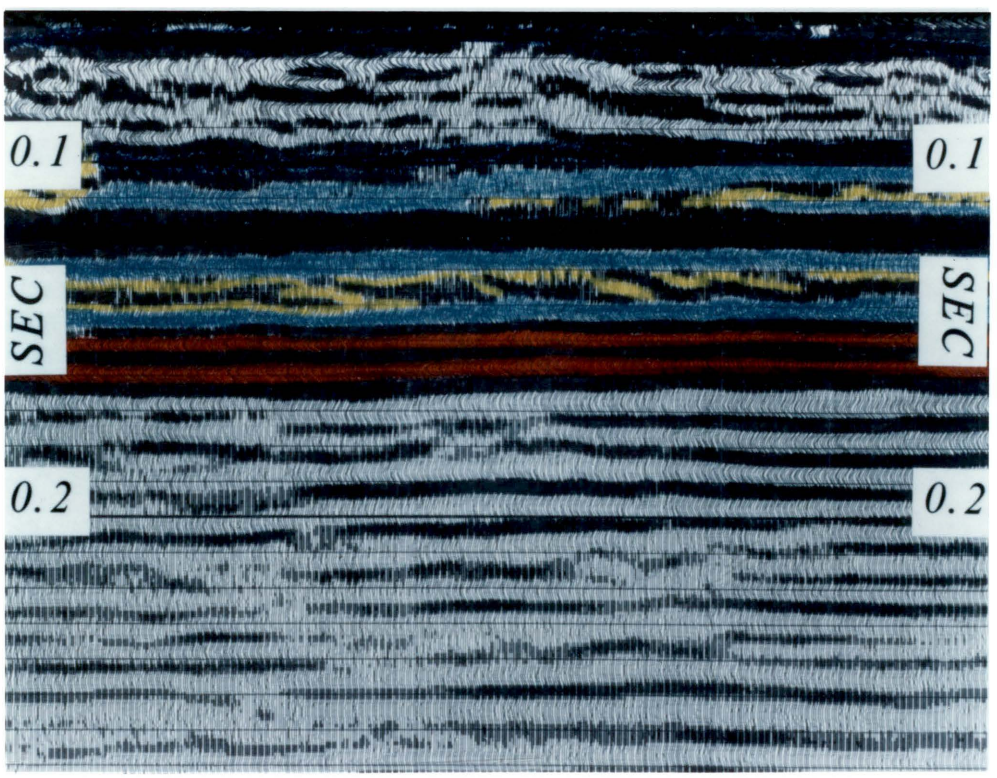
0.1
0.1
SEC
SEC
0.2
0.2

partially caused by differential compaction of the underlying shale and sand. Some of the structure may be due to velocity anomalies in the overlying glacial till, which have been identified from analysis of the stacking velocities. A Pleistocene channel or water saturated unconsolidated sediments, labelled A, at 30-60 msec from CDP 600 to 800 has been interpreted as the cause of the velocity pull-up adding apparent structure to the underlying marine sequence.

Three structures directly overlying the marine sequence at 120 msec have been interpreted as delta originating, clastic deposits. The deposits are labelled B and are located at CDP 440, 600, 800. A lack of erosional contact with the underlying marine horizon suggests conformable deposition of the sand which is characteristic of clastic deltaic deposits including distributary bar sands or levee deposits. The horizon is shown in detail in Figure 16.

Minor channel activity has been interpreted higher in the section and the channel development interrupts the marine sequences. Channels are apparent at 90 msec from CDP 440 to 600 and 105 msec from CDP 1000 to 1060. More minor channel development is interpreted from CDP 920 to 1060 at the horizon of major channel activity (135 msec). This may mark the waning phase of channel activity associated with this deltaic sequence. Directly to the east, overbank sands develop and show internal structure which may indicate foreset deposits of alternating sand and shale. This correlates with known current direction which has a component in an easterly direction. Detailed structure within the interpreted channel and overbank deposits are shown in Figure 17.


0.1
0.1
SEC
SEC
0.2
0.2

Figure 16. Deltaic deposits directly overlying marine event at 120 msec.

0.1
SEC
0.2
0.1
SEC
0.2

Figure 17. Internal structure of easternmost channel and overbank sands.

Normally flat lying and uniform events which are seen east of CDP 1150 show a definite variation in character to the west. This abrupt change in character probably indicates the eastern boundary of channel migration involving the upper Pennsylvanian sediments considered in this study. Because the region of channel activity varies rapidly from west to east (verified by hole information to the north - Appendix C), interpretation of shallow events (less than 100 msec) relies heavily upon correlation of waveform.

CONCLUSIONS

Geophysical techniques involving field acquisition and data processing have been modified to enhance and maintain high frequency content in the signal bandwidth. Single sweep processing has been employed to increase spatial sampling density and reduce low pass filtering associated with the array response. Whitening of the signal bandwidth has been accomplished using VSW during correlation and SAGC after correlation to further increase high frequency recovery. Spectral whitening improved data quality without the anticipated phase distortion associated conventional deconvolution filters. A wavelet-shaping filter was used to optimize the waveform length which allowed a thinner depositional sequence to be resolved. Static and dynamic corrections were applied to reduce the low pass filter effect after stack, and wave equation migration was used to remove diffracted energy from the section, especially within the channel areas.

Documented geological information concerning the transgressive-regressive deltaic environment was utilized to interpret events imaged in the section. Where available, test hole information was used to verify waveform shapes associated with geological horizons.

The high resolution data acquisition and processing led to an interpreted section which shows cyclic deposition in a deltaic environment. Complex channel development interrupted the underlying Herrin coal seam complex. Contrary to previous interpretations of the channel location

by Chapman and others (1981), and Nelson (1983), the channel can faithfully be interpreted as having bimodal structure leaving an "island" of undisturbed deposits. Channel activity effects the younger Pennsylvanian sediments and also the unconsolidated Pleistocene till as well. A limit to the eastern migration of channel development affecting the the Pennsylavanian sediments considered in this study can be identified by the abrupt change in event characteristics.

REFERENCES

Anderson, M. J., 1961, Geology and petrology of the Trivoli Sandstone in the Illinois Basin, Illinois State Geological Circular 316, 31 p.

Angeleri, G. P., Loinger, E., 1984, Phase distortion due to absorption in seismograms and vsp, Geophysical Prospecting, Vol. 32, p. 406-424.

Applegate, J. K., Emilia, D. A., Neitzel, E. B., and Donaldson, P. R.,1982, High-resolution seismic study in the Gas Hills uranium district, Wyoming, Geophysics, Vol. 47, No. 10, p. 1355-1374.

Belcher, S. W., 1984,Spacial resolution by single sweep recording and processing, Master's Thesis, Virginia Tech.

Berkhout, A. J., 1984, Seismic Resolution, Resolving Power of Acoustical Echo Techniques, Handbook of Geophysical Exploration, Vol. 12, Geophysical Press, 228 p.

Chapman, W. L., Brown, G. L., Fair D. W., 1981, The Vibroseis system, a high-frequency tool, Geophysics, Vol. 46, ?-? p.

Coruh, C., 1985, Streched automatic amplitude adjustment of seismic data, Geophysics, 50, No. 2, p. 252-256.

Coruh, C., and Costain, J. K., 1983, Noise attenuation by Vibroseis whitening(vsw) processing, Geophysics, 48, p. 252-256.

Gibson, B., Larner, K., 1984, Predictive deconvolution and the zero phase source, Geophysics, Vol. 49, No. 4, p. 379-397.

Hoover, G. M., Gallagher, J. G., Rigdon, H. K., 1984, Vibrator Signals, Proceedings of the IEEE, Vol. 72, No. 10, pp. 1290-11301.

Hopkins, M. E., Nance, R. B., Treworgy, C. G., 1979, Mining geology of Illinois coal deposits, in, Depositional and Structural History of the Pennsylvanian System of the Illinois Basin, Part 2, pp. 142-151.

Koefoed, O., 1981, Aspects of vertical seismic resolution, Geophysical Prospecting, Vol. 29, pp. 21-30.

Neidell, N. S., Poggiaglioimi, E., 1977, Stratigraphic modeling and interpretation- geophysical principles and techniques, in Payton,

C. E.,(ed.), Seismic Stratigraphy - Applications to Hydrocarbon Exploration, AAPG Memoir No. 26, p. 389-416.

Nelson, J. W., 1983, Geologic disturbances in Illinois coal seams, Illinois State Geological Survey, Circ. 530, ?? p.

Palmer, J. E., Jacobson, R. J., Trask, C. B., 1979, Deposition of strata of Late Desmoinesian Age overlying the Herrin(no. 6) Coal Member in Southwestern Illinois, in, Depositional and Structural History of the Pennsylvanian System of the Illinois Basin, Part 2, p. 92-102.

Potter, P. E., and Simon, J. A., 1961, Anvil Rock Sandstone and channel cutouts of Herrin(no. 6) Coal in west-central Illinois, Illinois state Geological Survey Circ. 314, 12 p.

Schoenberger, M., 1974, Resolution comparison of minimum-phase and zero phase signals, Geophysics, Vol. 39, No. 6, p. 826-833.

Sheriff, R. E., Geldart, L. P., 1982, Exploration Seismology, Vol. 1, History, Theory, and Data Acquisition, Cambridge University Press, 253 p.

Sheriff, R. E., Geldart, L. P., 1983, Exploration Seismology, Vol. 2, Data Processing and Interpretation, Cambridge University Press, 221 p.

Wanless, H. R., Bariffio, J. R., Trescott, P. R., 1969, Conditions of deposition of Pennsylvanian coal beds, in E. C. Dapples and M. E. Hopkins(eds.), Environments of Coal Deposition, GSA Special Paper 114, p. 105-142.

Wanless, H. R., Baroffio, J. R., Rocha-Campos, A., Horne, J. C., Orlopp, D. E., Trescott, P. R., Vail, R. S., and Wright, C. R., 1970, Late Paleozoic deltas in the central and eastern United States, in J. P. Morgan,(ed.), Deltaic Sedimentation, Modern and Ancient, SEPM Special Publication 15, p. 215-245.

Willman, H. B., et al, 1975, Handbook of Illinois stratigraphy, Illinois State Geological Society, Bul. 95, 261 p.

Waters, K. E., 1981, Reflection Seismology, John Wiley and Sons, 261 p.

Ziolkowski, A., Lerwill, W. E.,1979,A simple aproach to high resolution seismic profiling for coal, Geophysical Prospecting, Vol. 27, 39 p.

APPENDIX A - ARRAY RESPONSE

Field arrays are designed to attenuate longitudinal surface wave energy which is recorded as coherent noise. Near surface reflectors return energy to the surface with finite apparent velocities. High frequency components of the reflected signal are subject to filtering if the array parameters are not carefully selected.

The frequency response of source and receiver arrays can be determined in a similar fashion. The total system array response is calculated using a convolutional model in the time domain or complementary multiplication in the frequency domain.

A single raypath model is shown in Figure A1 where a wavefront is incident upon a surface array (source or receiver) with angle, α.

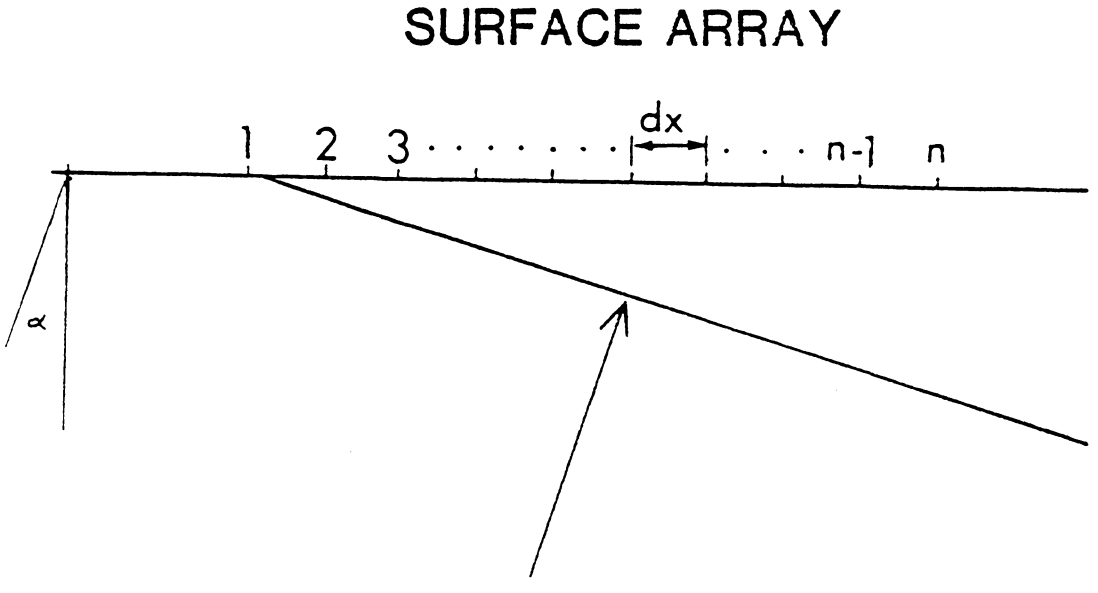

Figure A1. INCIDENT RAYPATH

The surface array is defined to have n elements and an element spacing of dx. The impulse response of the array is given by;

$$R(x) = \sum_{i=1}^{n} A_i * \alpha(x - x_i)$$

where A is a weighting coefficient for the elements. With uniform weighting, the coefficient is unity for i=1,n. The discrete Fourier transform of the impulse response is;

$$R(f) = \sum_{i=1}^{n} e^{-j2\pi x_i f \sin\alpha / V}$$

where f is the frequency component of the signal and V is the velocity of the near surface layer. Normalizing the response and rewriting the exponential as a trigonometric expression;

$$R(f) = 1/n\{ \sum_{i=1}^{n} [\cos(2\pi(i-1)dxf\sin\alpha/V)^2 - j\sin(2\pi(i-1)dxf\sin\alpha/V)^2]\}^{\frac{1}{2}}$$

Assuming linear theory, the total system response is the frequency domain multiplication of the source and receiver response.

$$TR(f)= 1/n\{ \sum_{i=1}^{n} [\cos(2\pi(i-1)dgf\sin\alpha/V)^2 - j\sin(2\pi(i-1)dgf\sin\alpha/V)^2]\}^{\frac{1}{2}} *$$

$$1/m\{ \sum_{i=1}^{m} [\cos(2\pi(i-1)dsf\sin\alpha/V)^2 - j\sin(2\pi(i-1)dsf\sin\alpha/V)^2]\}^{\frac{1}{2}}$$

where;

n= no. of receiver elements m= no. of source elements

dg= receiver el. spacing ds= source el. spacing

α=incident angle of wavefront V=near surface velocity

Frequency response curves relating specifically to the geometry of the seismic line in this study are given. The frequency response to surface wave energy, i.e., α=90 deg, with velocity of 700 m/sec is shown in Figure A2. For reflected energy with an incident angle of α=9 deg, the frequency response to the apparent surface energy (2300 m/sec - V(app)=V/sinα) is shown in Figure A3. Note that the 20-element array attenuates surface wave energy in the frequency band of 80-100 Hz while the 2-element arrays do not. The 20-element response to apparent velocity shows attenuation of high frequencies in the signal bandwidth and the 2-element arrays do not attenuate the frequencies as severely. By processing the data using the 2-element source arrays, the data is not affected by the more severe low pass filter attributed to the 20-element source array.

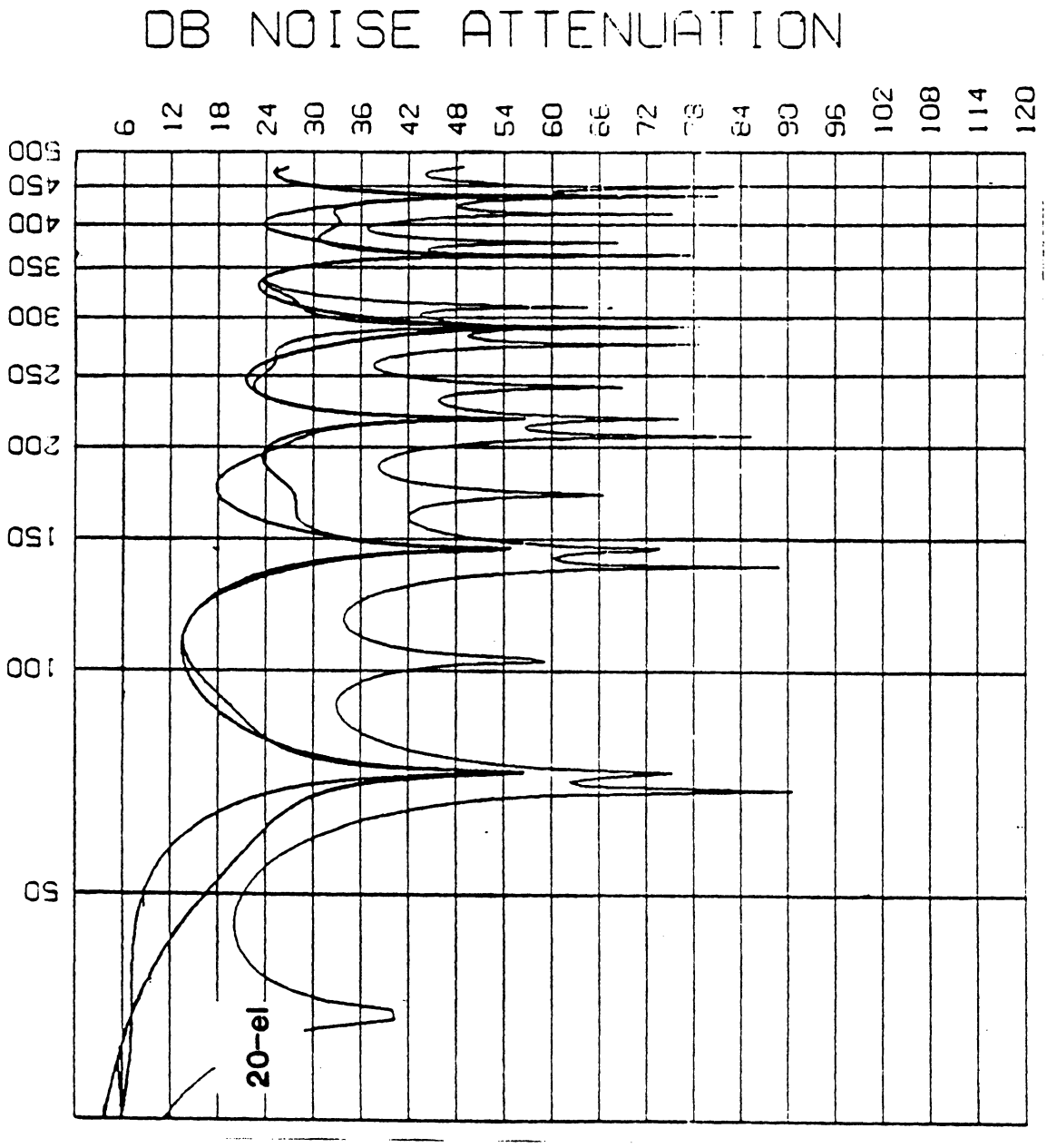

Figure A2. Frequency response for surface wave energy.

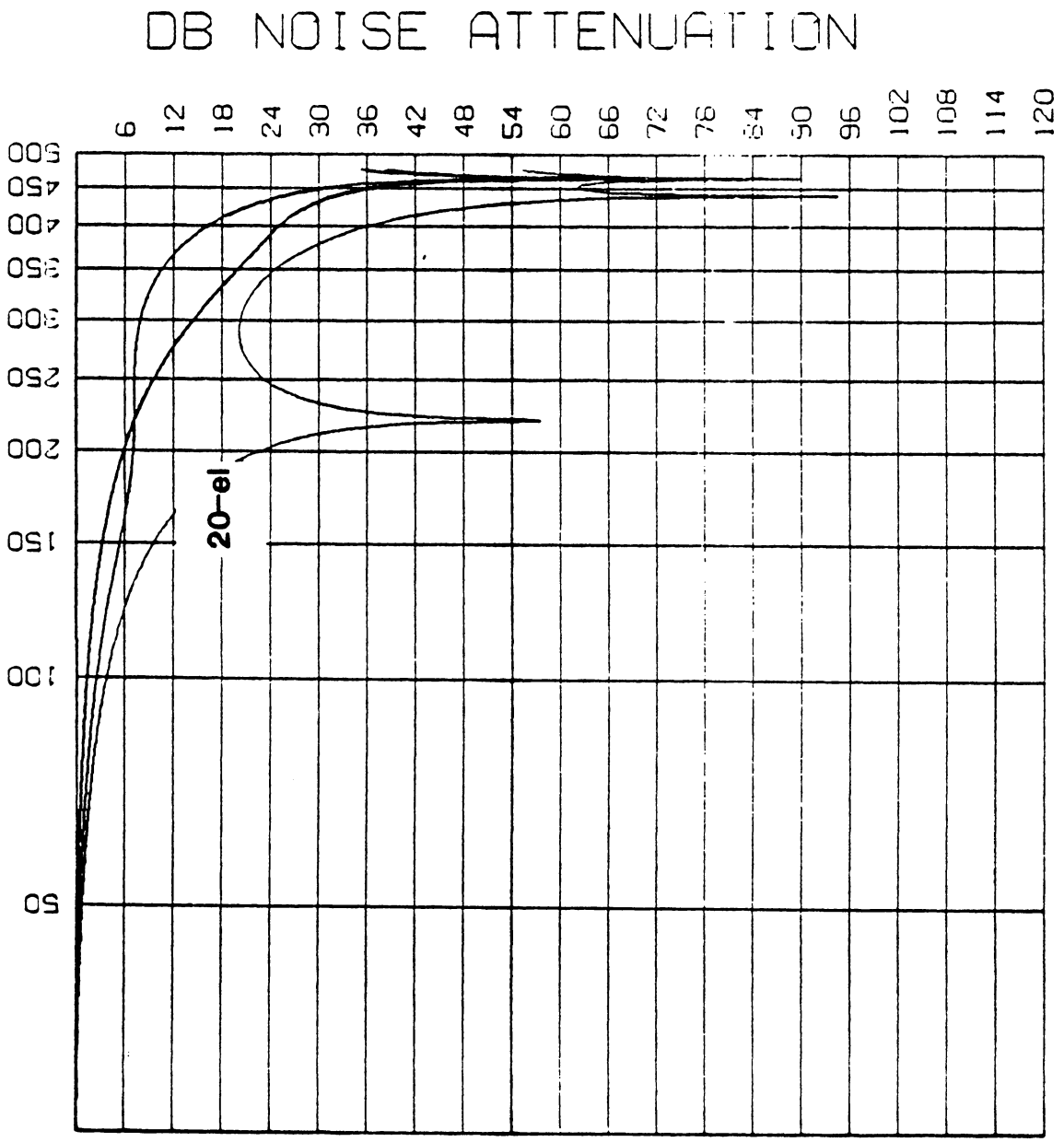

Figure A3. Frequency response for incident energy.

APPENDIX B - STACKING VELOCITIES

Table 3. Stacking Velocities

	VELOCITY INFORMATION FOR CDP 150				
T(tot) SEC	Stacking Velocity M/SEC	Interval Velocity M/SEC	T(int) SEC	Average Velocity M/SEC	Depth M
		1158	0.033		
0.033	1158	1495	0.024	1158	19
0.057	1311	1936	0.015	1300	37
0.072	1463	2771	0.020	1432	52
0.092	1829	2322	0.048	1723	79
0.140	2012	2996	0.016	1929	135
0.156	2134	4155	0.024	2038	159
0.180	2499	3203	0.015	2320	209
0.195	2560	3937	0.015	2388	233
0.210	2682			2499	262

	VELOCITY INFORMATION FOR CDP 250				
T(tot) SEC	Stacking Velocity M/SEC	Interval Velocity M/SEC	T(int) SEC	Average Velocity M/SEC	Depth M
		914	0.000		
0.000	914	1128	0.030	914	0
0.030	1128	1481	0.040	1128	17
0.070	1341	2128	0.035	1330	47
0.105	1646	1869	0.037	1596	84
0.142	1707	4181	0.018	1667	118
0.160	2134	3032	0.034	1950	156
0.194	2316	2682	0.036	2140	208
0.230	2377			2225	256

	VELOCITY INFORMATION FOR CDP 350				
T(tot) SEC	Stacking Velocity M/SEC	Interval Velocity M/SEC	T(int) SEC	Average Velocity M/SEC	Depth M
		1189	0.031		
0.031	1189	1335	0.021	1189	18
0.052	1250	1375	0.016	1248	32
0.068	1280	2831	0.017	1277	43
0.085	1707	3412	0.016	1588	67
0.101	2073	2432	0.019	1877	95
0.120	2134	2501	0.022	1965	118
0.142	2195	2542	0.028	2048	145
0.170	2256	2886	0.016	2129	181
0.186	2316	3856	0.019	2194	204
0.205	2499			2348	241

	VELOCITY INFORMATION FOR CDP 450				
T(tot) SEC	Stacking Velocity M/SEC	Interval Velocity M/SEC	T(int) SEC	Average Velocity M/SEC	Depth M
		1219	0.039		
0.039	1219	1427	0.015	1219	24
0.054	1280	1430	0.013	1277	34
0.067	1311	1426	0.023	1307	44
0.090	1341	3136	0.004	1337	60
0.094	1463	4079	0.020	1414	66
0.114	2164	2793	0.032	1881	107
0.146	2316	2824	0.018	2081	152
0.164	2377	2992	0.016	2162	177
0.180	2438			2236	201

	VELOCITY INFORMATION FOR CDP 550				
T(tot) SEC	Stacking Velocity M/SEC	Interval Velocity M/SEC	T(int) SEC	Average Velocity M/SEC	Depth M
		1219	0.047		
0.047	1219	1648	0.016	1219	29
0.063	1341	2609	0.014	1328	42
0.077	1646	2215	0.018	1561	60
0.095	1768	3256	0.025	1685	80
0.120	2164	2312	0.030	2012	121
0.150	2195	3628	0.020	2072	155
0.170	2408	2408	0.025	2055	192
0.195	2408			2275	222

	VELOCITY INFORMATION FOR CDP 650				
T(tot) SEC	Stacking Velocity M/SEC	Interval Velocity M/SEC	T(int) SEC	Average Velocity M/SEC	Depth M
		1189	0.030		
0.030	1189	1317	0.026	1189	18
0.056	1250	2019	0.034	1248	35
0.090	1585	3353	0.014	1539	69
0.104	1920	3000	0.024	1784	93
0.128	2164	2339	0.026	2012	129
0.154	2194	3131	0.031	2067	159
0.185	2377	3299	0.011	2245	208
0.196	2438			2304	226

	VELOCITY INFORMATION FOR CDP 750				
T(tot) SEC	Stacking Velocity M/SEC	Interval Velocity M/SEC	T(int) SEC	Average Velocity M/SEC	Depth M
		914	0.000		
0.000	914	1128	0.030	914	0
0.030	1128	1155	0.026	1128	17
0.056	1189	1468	0.014	1187	33
0.070	1250	1950	0.036	1243	44
0.106	1524	2717	0.020	1483	79
0.126	1768	3923	0.024	1679	106
0.150	2256	2731	0.020	2038	153
0.170	2316	3115	0.012	2120	180
0.182	2377	2731	0.016	2185	199
0.198	2408			2229	221

	VELOCITY INFORMATION FOR CDP 850				
T(tot) SEC	Stacking Velocity M/SEC	Interval Velocity M/SEC	T(int) SEC	Average Velocity M/SEC	Depth M
		1189	0.030		
0.030	1189	1899	0.065	1189	18
0.095	1707	1877	0.020	1675	80
0.115	1733	2680	0.022	1710	98
0.137	1920	4259	0.018	1865	128
0.155	2316	3455	0.015	2143	166
0.170	2438	3147	0.014	2259	192
0.184	2499	3423	0.011	2327	214
0.195	2560			2389	233

	VELOCITY INFORMATION FOR CDP 950				
T(tot) SEC	Stacking Velocity M/SEC	Interval Velocity M/SEC	T(int) SEC	Average Velocity M/SEC	Depth M
		914	0.000		
0.000	914	1158	0.039	914	0
0.038	1158	1263	0.015	1158	22
0.053	1189	1600	0.013	1188	31
0.066	1280	2123	0.014	1269	42
0.080	1463	1937	0.024	1418	57
0.104	1585	3986	0.016	1538	80
0.120	2073	3326	0.010	1864	112
0.130	2195	3162	0.025	1977	128
0.155	2377	3912	0.016	2168	168
0.171	2560			2331	199

	VELOCITY INFORMATION FOR CDP 1050				
T(tot) SEC	Stacking Velocity M/SEC	Interval Velocity M/SEC	T(int) SEC	Average Velocity M/SEC	Depth M
		1128	0.035		
0.035	1128	1541	0.032	1128	20
0.067	1341	2766	0.014	1325	44
0.081	1676	1831	0.019	1574	64
0.100	1707	2772	0.016	1623	81
0.116	1890	3441	0.039	1781	103
0.155	2377	3249	0.035	2199	170
0.190	2560			2392	227

	VELOCITY INFORMATION FOR CDP 1150				
T(tot) SEC	Stacking Velocity M/SEC	Interval Velocity M/SEC	T(int) SEC	Average Velocity M/SEC	Depth M
		914	0.000		
0.000	914	1341	0.064	914	0
0.064	1341	2165	0.021	1341	43
0.085	1585	2526	0.016	1545	66
0.101	1768	2724	0.019	1700	86
0.120	1951	2272	0.026	1862	112
0.146	2012	6563	0.004	1935	141
0.150	2256	3566	0.012	2059	154
0.162	2377	3725	0.006	2170	176
0.168	2438			2226	187

	VELOCITY INFORMATION FOR CDP 1350				
T(tot) SEC	Stacking Velocity M/SEC	Interval Velocity M/SEC	T(int) SEC	Average Velocity M/SEC	Depth M
		914	0.000		
0.000	914	975	0.060	914	0
0.060	975	2880	0.025	975	29
0.085	1768	2423	0.028	1538	65
0.113	1951	2555	0.011	1757	99
0.124	2012	3062	0.013	1828	113
0.137	2134	3267	0.021	1945	133
0.158	2316	3244	0.020	2121	168
0.178	2438			2247	200

	VELOCITY INFORMATION FOR CDP 1550				
T(tot) SEC	Stacking Velocity M/SEC	Interval Velocity M/SEC	T(int) SEC	Average Velocity M/SEC	Depth M
		1219	0.000		
0.000	914	1648	0.065	914	0
0.065	1341	2609	0.033	1341	44
0.098	1768	2215	0.012	1696	83
0.110	1951	3256	0.008	1845	101
0.118	2012	2312	0.017	1904	112
0.135	2134	3628	0.015	2022	136
0.150	2256	2408	0.008	2134	160
0.158	2377	2408	0.042	2230	172
0.200	2682			2519	252

	VELOCITY INFORMATION FOR CDP 1750				
T(tot) SEC	Stacking Velocity M/SEC	Interval Velocity M/SEC	T(int) SEC	Average Velocity M/SEC	Depth M
		914	0.000		
0.000	914	975	0.060	914	0
0.060	975	1924	0.002	975	29
0.080	1280	3362	0.020	1212	48
0.100	1890	2535	0.020	1642	82
0.120	2012	3662	0.015	1791	107
0.135	2256	2731	0.018	1999	135
0.153	2316	2868	0.017	2085	160
0.170	2778	3545	0.016	2163	184
0.186	2499			2282	212

	VELOCITY INFORMATION FOR CDP 1950				
T(tot) SEC	Stacking Velocity M/SEC	Interval Velocity M/SEC	T(int) SEC	Average Velocity M/SEC	Depth M
		1219	0.000		
0.000	914	1427	0.063	914	0
0.063	1280	1430	0.017	1280	40
0.080	1463	1426	0.014	1433	57
0.094	1524	3136	0.012	1493	70
0.106	1890	4079	0.014	1737	92
0.120	2225	2793	0.030	1993	120
0.150	2256	2824	0.024	2069	155
0.174	2438	2992	0.026	2247	196
0.200	2682			2468	247

APPENDIX C - WELL INFORMATION

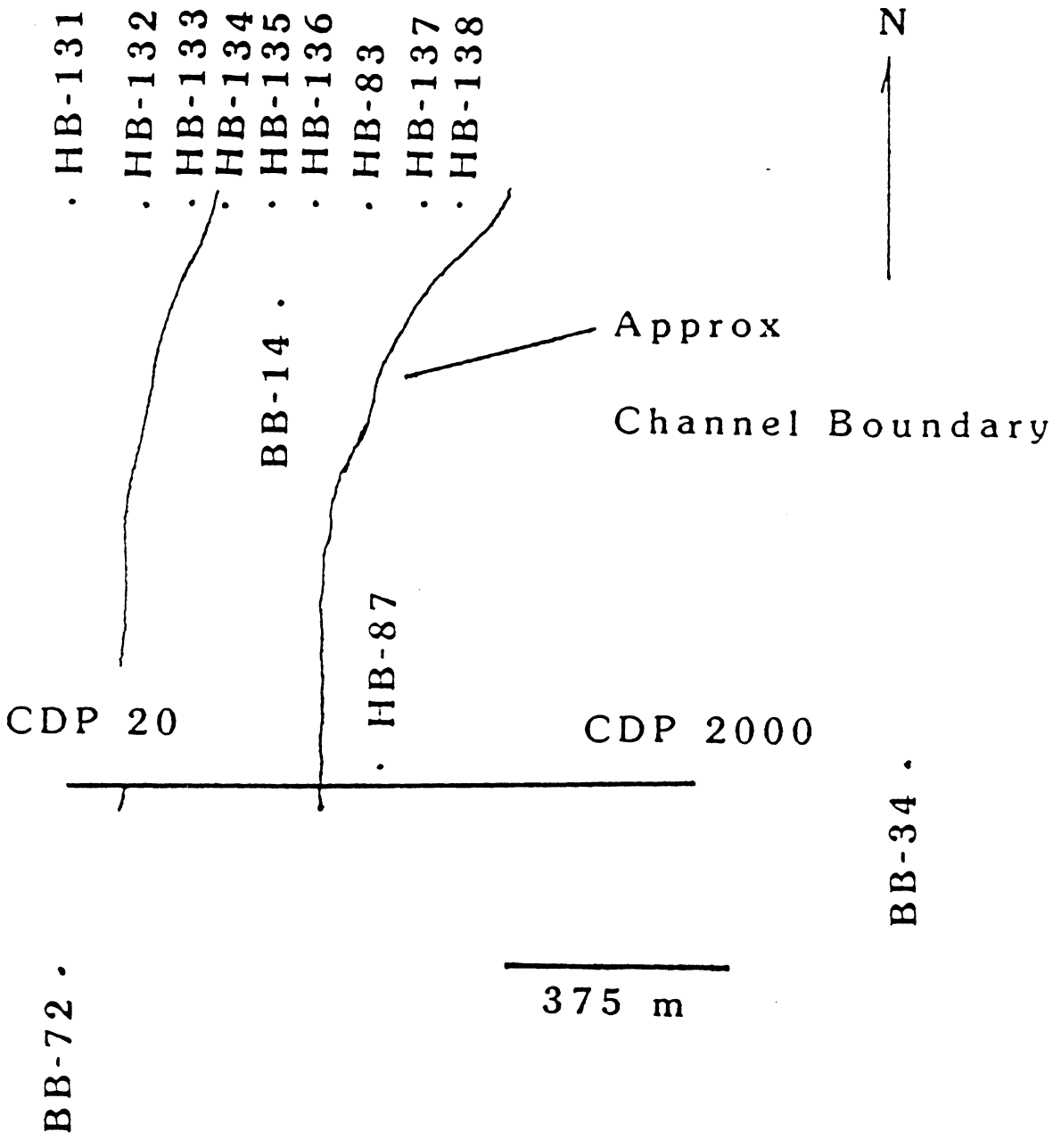

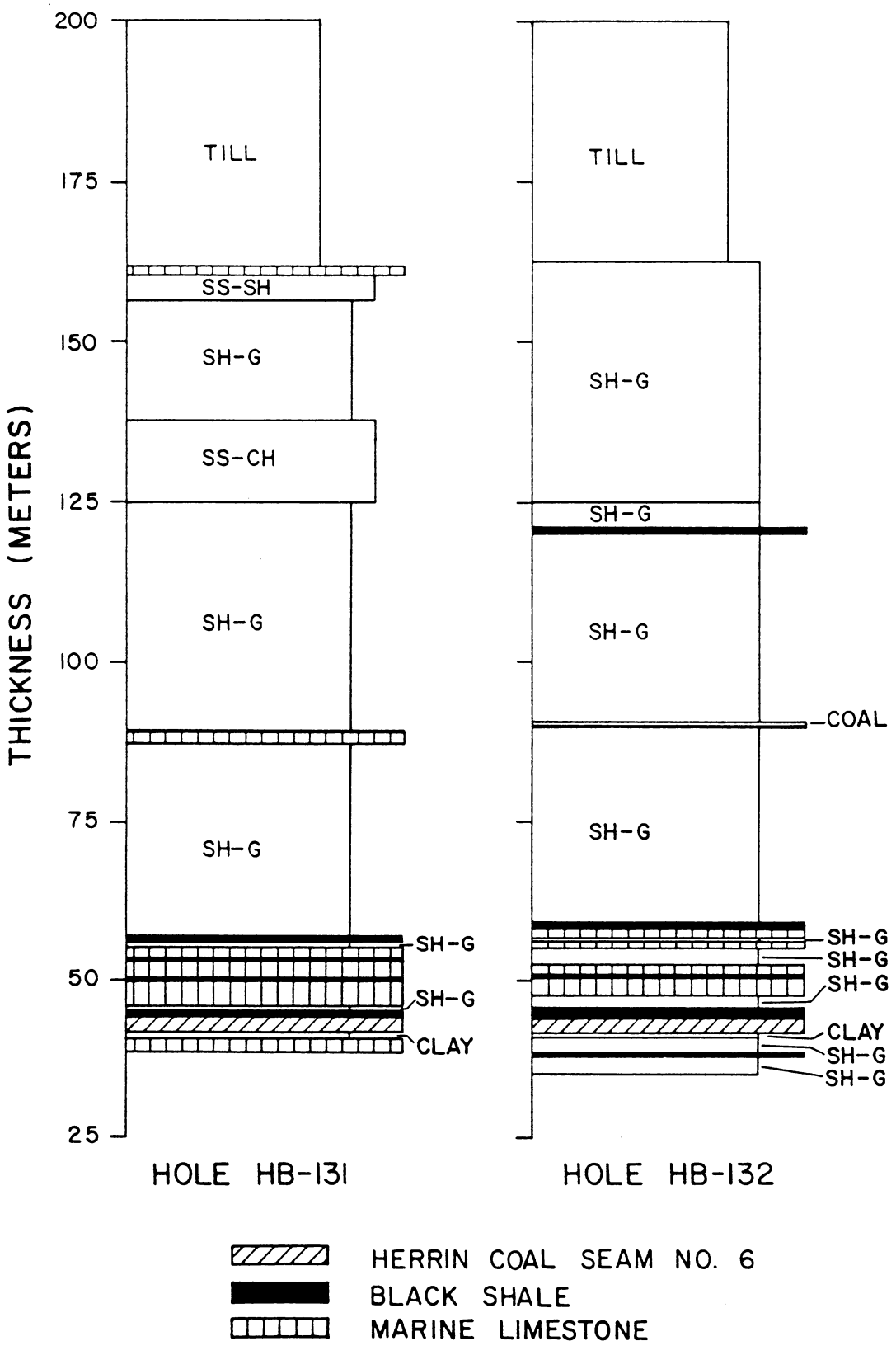
200
175
150
125
100
75
50
25
THICKNESS (METERS)
TILL
SS-SH
SH-G
SS-CH
SH-G
SH-G
CLAY
HOLE HB-131
TILL
SH-G
SH-G
COAL
SH-G
SH-G
SH-G
SH-G
CLAY
SH-G
SH-G
HOLE HB-132
HERRIN COAL SEAM NO. 6
BLACK SHALE
MARINE LIMESTONE

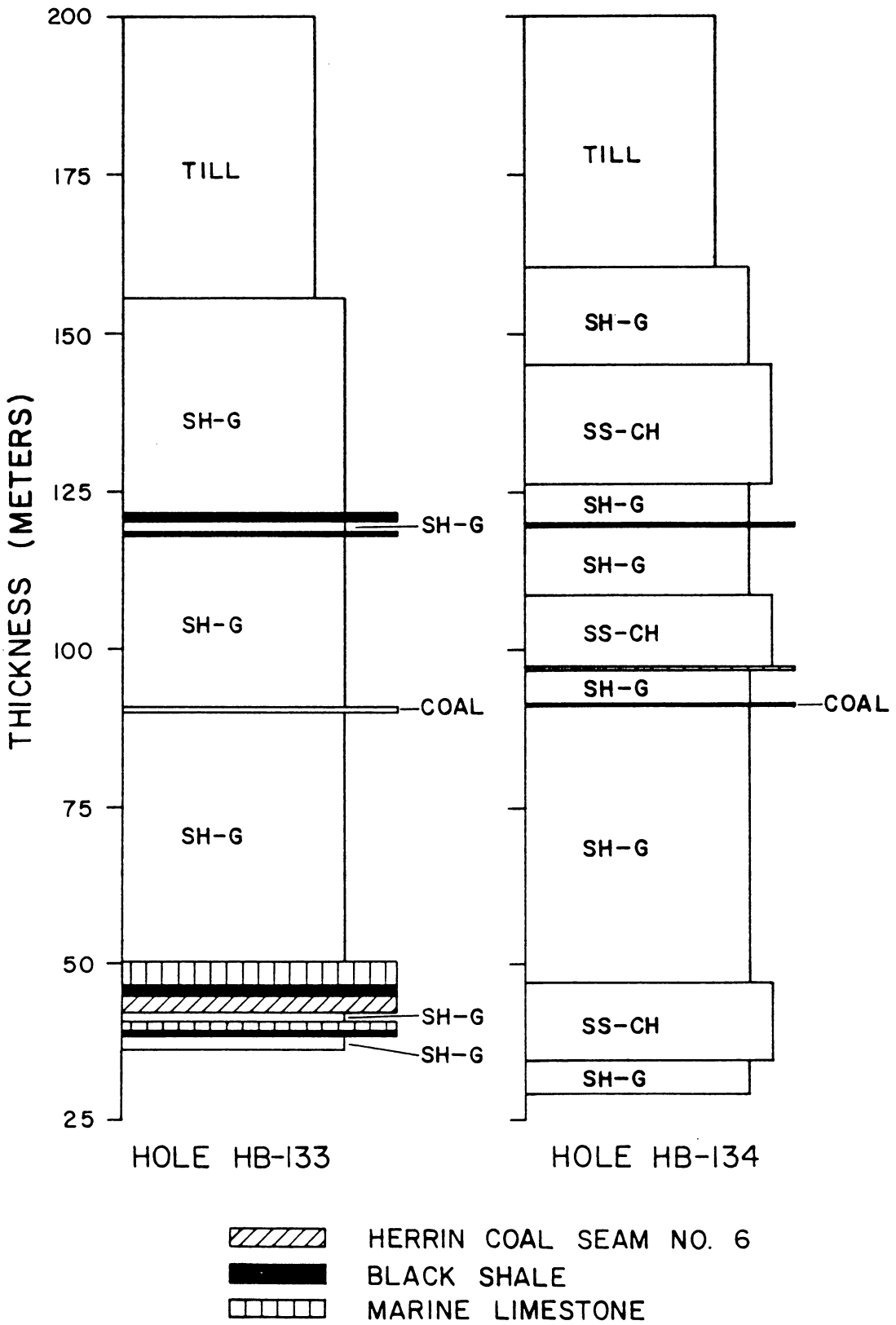
200
175
150
125
100
75
50
25
THICKNESS (METERS)
TILL
SH-G
SH-G
SH-G
COAL
SH-G
SH-G
SH-G
HOLE HB-133
TILL
SH-G
SS-CH
SH-G
SH-G
SS-CH
SH-G
COAL
SH-G
SS-CH
SH-G
HOLE HB-134
HERRIN COAL SEAM NO. 6
BLACK SHALE
MARINE LIMESTONE

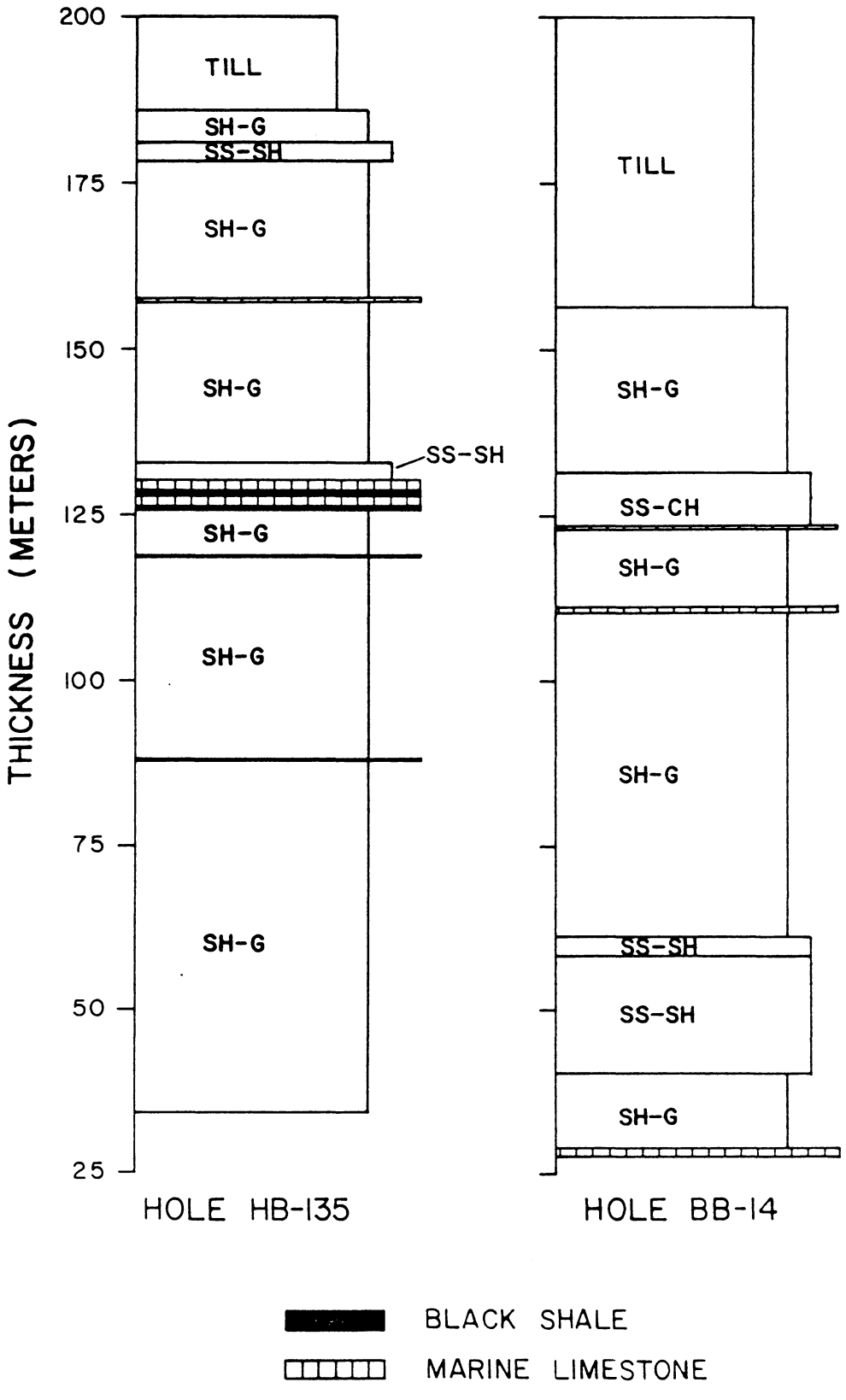
200
175
150
125
100
75
50
25
THICKNESS (METERS)
TILL
SH-G
SS-SH
SH-G
SH-G
SS-SH
SH-G
SH-G
SH-G
HOLE HB-135
TILL
SH-G
SS-CH
SH-G
SH-G
SS-SH
SS-SH
SH-G
HOLE BB-14
BLACK SHALE
MARINE LIMESTONE

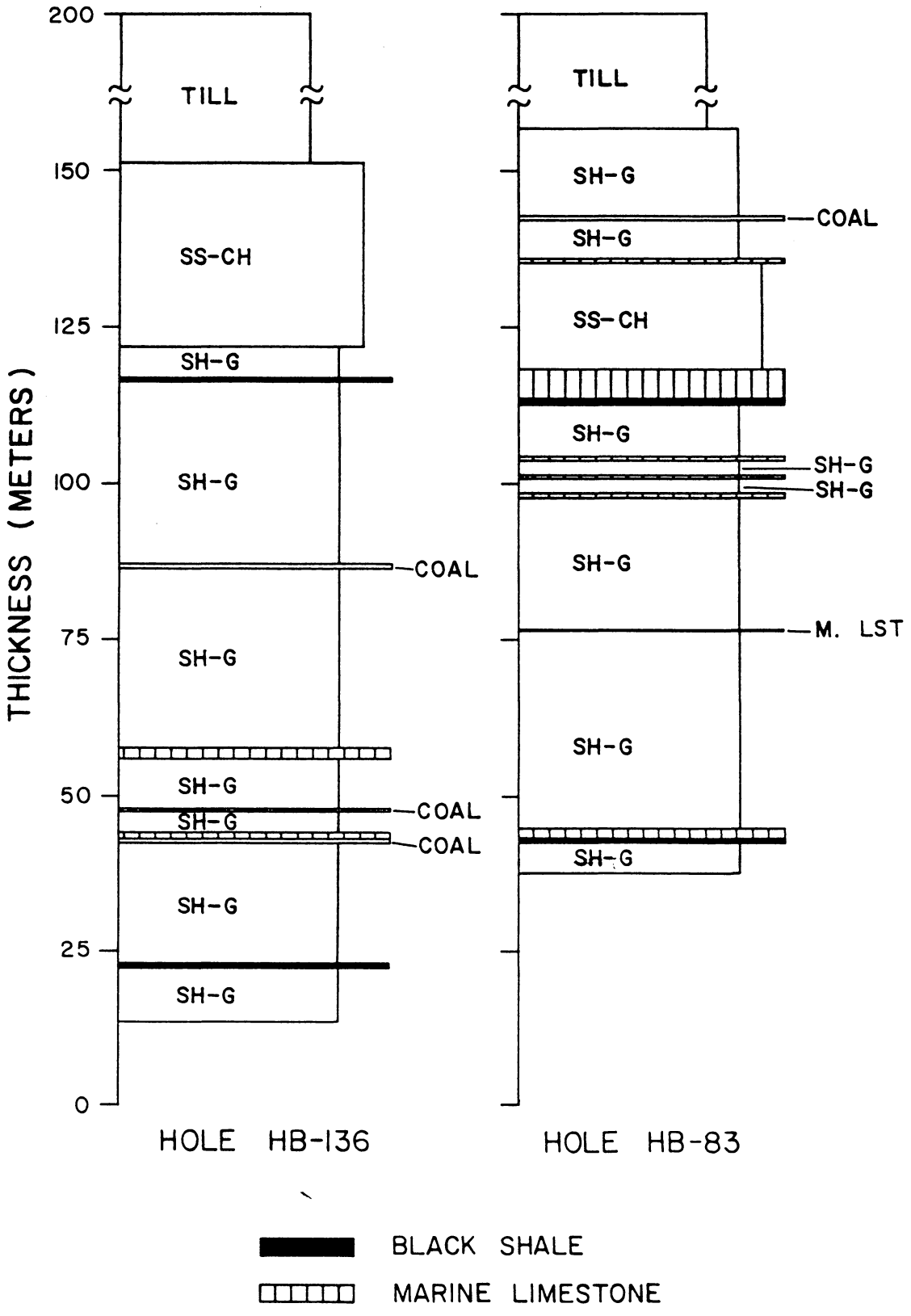
200
150
125
100
75
50
25
0
THICKNESS (METERS)
TILL
SS-CH
SH-G
SH-G
COAL
SH-G
SH-G
COAL
SH-G
COAL
SH-G
SH-G
HOLE HB-136
TILL
SH-G
COAL
SH-G
SS-CH
SH-G
SH-G
SH-G
SH-G
M. LST
SH-G
SH-G
HOLE HB-83
BLACK SHALE
MARINE LIMESTONE

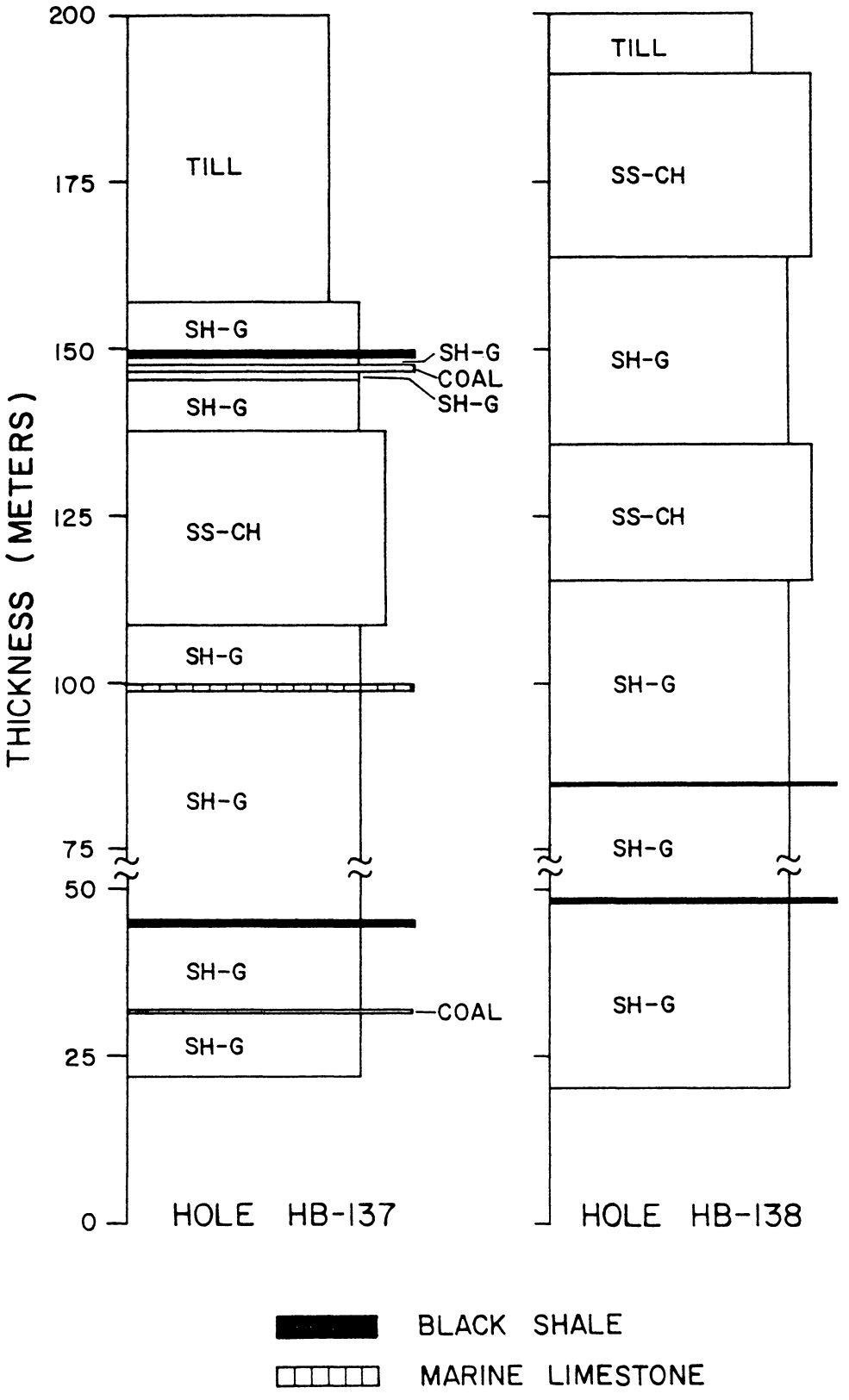
200
175
150
125
100
75
50
25
0
THICKNESS (METERS)
TILL
SH-G
SH-G
COAL
SH-G
SH-G
SS-CH
SH-G
SH-G
SH-G
COAL
SH-G
HOLE HB-137
TILL
SS-CH
SH-G
SS-CH
SH-G
SH-G
SH-G
HOLE HB-138
BLACK SHALE
MARINE LIMESTONE

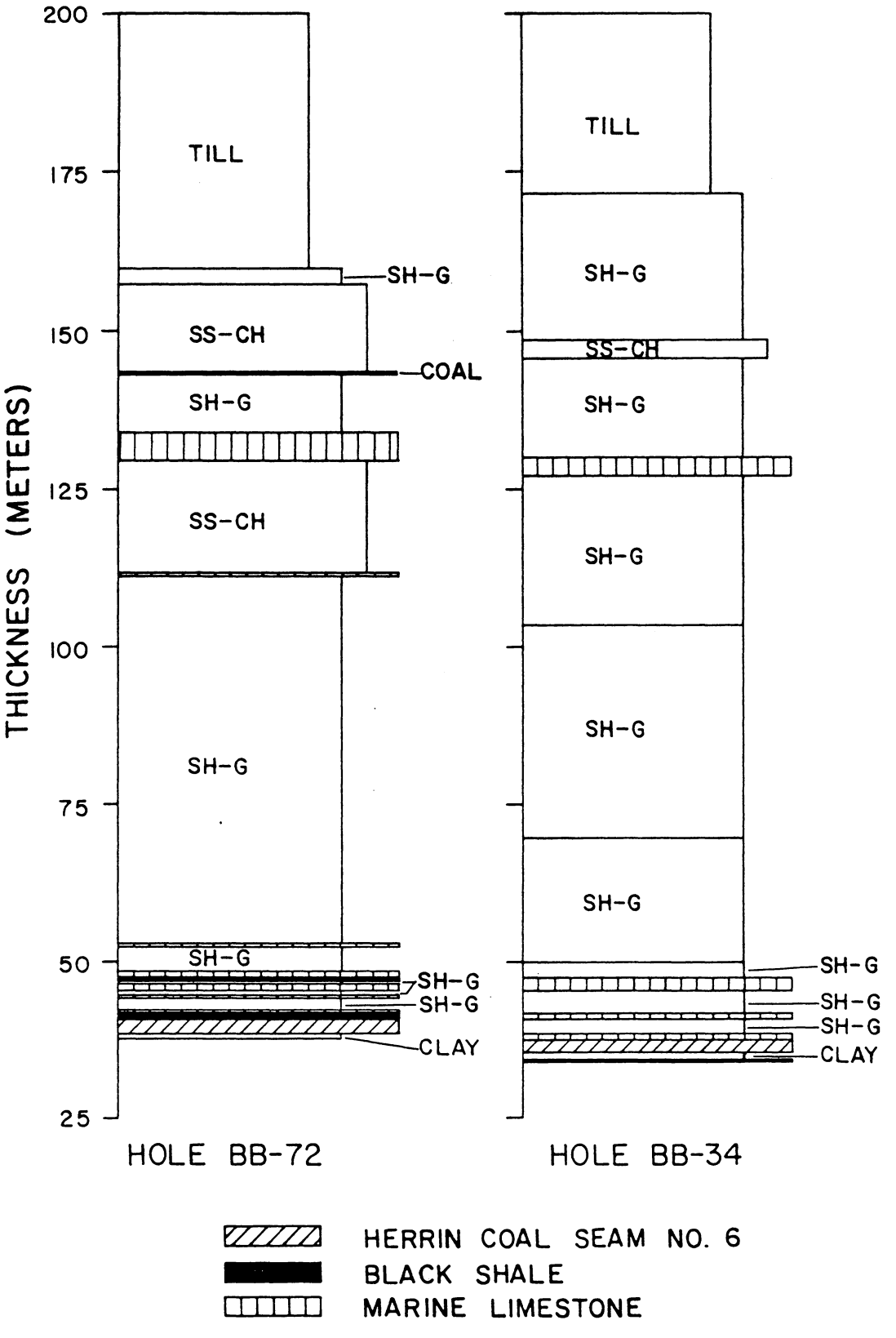
200
175
150
125
100
75
50
25
THICKNESS (METERS)
TILL
SH-G
SS-CH
COAL
SH-G
SS-CH
SH-G
SH-G
SH-G
SH-G
CLAY
HOLE BB-72
TILL
SH-G
SS-CH
SH-G
SH-G
SH-G
SH-G
SH-G
SH-G
SH-G
CLAY
HOLE BB-34
HERRIN COAL SEAM NO. 6
BLACK SHALE
MARINE LIMESTONE

The vita has been removed from the scanned document

W

91.5 m

FINAL MIGRATED STACKED SECTION

E

CDP

CDP 200 400 600 800 1000 1200 1400 1600 1800 2000

CDP-STAT

0.00

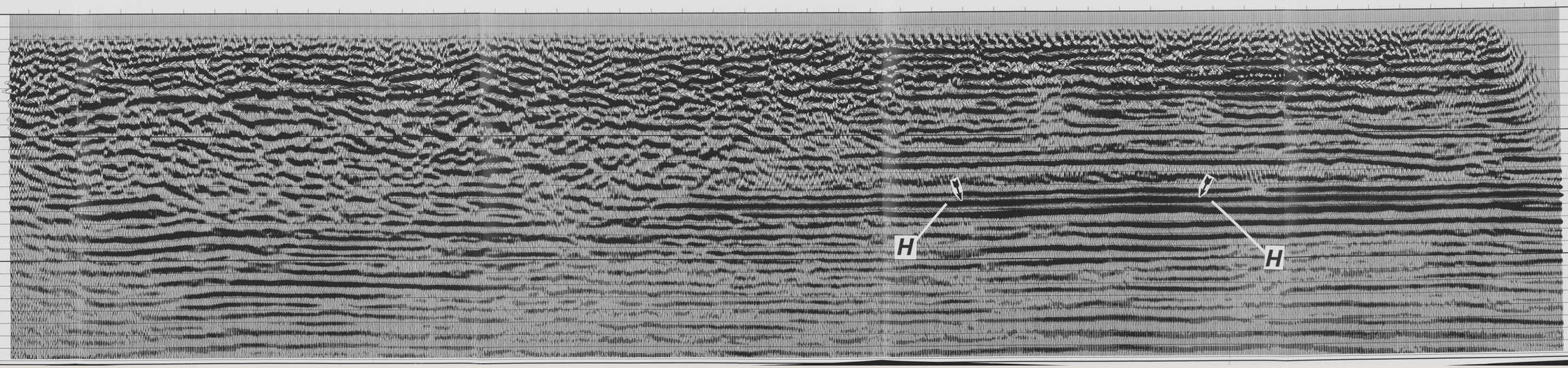

W

91.5 m

INTERPRETIVE STACKED SECTION

HERRIN COAL COMPLEX
MARINE DEPOSITS
SANDSTONE
DELTAIC SHALE
UNCONFORMITY BOUNDARY

E

CDP

CDP 200 400 600 800 1000 HB-87 1200 1400 1600 2000

CDP-STAT

0.00 0.0

TIME SEC

0.1

0.2

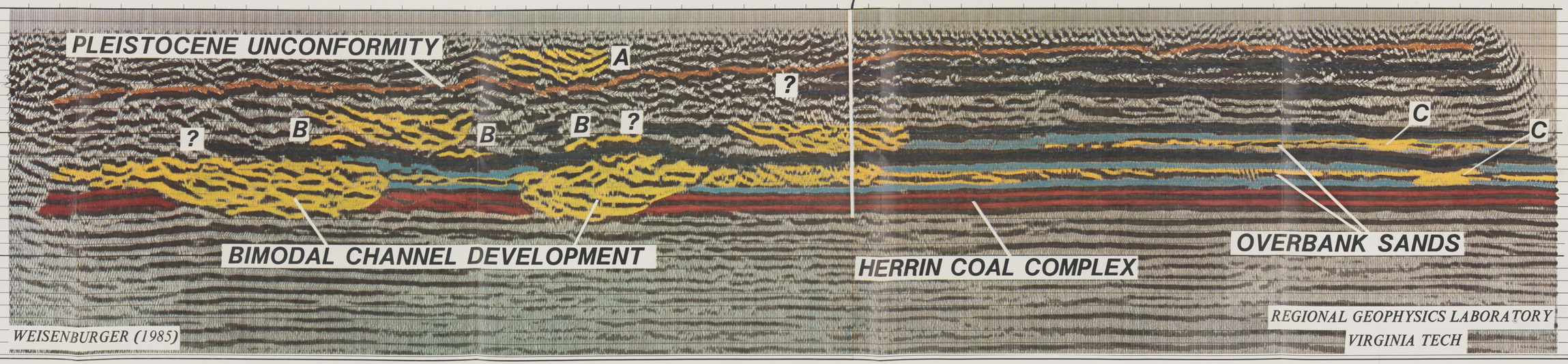

WEISENBURGER (1985)

REGIONAL GEOPHYSICS LABORATORY
VIRGINIA TECH